Neurobiology of Disease

Dysregulated RNA-Induced Silencing Complex (RISC) Assembly within CNS Corresponds with Abnormal miRNA Expression during Autoimmune Demyelination

Przemysław Lewkowicz, Hanna Cwiklińska, Marcin P. Mycko, Maria Cichalewska, Małgorzata Domowicz, Natalia Lewkowicz, Anna Jurewicz, and Krzysztof W. Selmaj

Department of Neurology, Laboratory of Neuroimmunology, Medical University of Lodz, 92-213 Lodz, Poland

MicroRNAs (miRNAs) associate with Argonaute (Ago), GW182, and FXR1 proteins to form RNA-induced silencing complexes (RISCs). RISCs represent a critical checkpoint in the regulation and bioavailability of miRNAs. Recent studies have revealed dysregulation of miRNAs in multiple sclerosis (MS) and its animal model, experimental autoimmune encephalomyelitis (EAE); however, the function of RISCs in EAE and MS is largely unknown. Here, we examined the expression of Ago, GW182, and FXR1 in CNS tissue, oligodendrocytes (OLs), brain-infiltrating T lymphocytes, and CD3$^+$ splenocytes (SCs) of EAE mic, and found that global RISC protein levels were significantly dysregulated. Specifically, Ago2 and FXR1 levels were decreased in OLs and brain-infiltrating T cells in EAE mice. Accordingly, assembly of Ago2/GW182/FXR1 complexes in EAE brain tissues was disrupted, as confirmed by immunoprecipitation experiments. In parallel with alterations in RISC complex content in OLs, we found downregulation of miRNAs essential for differentiation and survival of OLs and myelin synthesis. In brain-infiltrating T lymphocytes, aberrant RISC formation contributed to miRNA-dependent proinflammatory helper T-cell polarization. In CD3$^+$ SCs, we found increased expression of both Ago2 and FXR1 in EAE compared with nonimmunized mice. Therefore, our results demonstrate a gradient in expression of miRNA between primary activated T cells in the periphery and polarized CNS-infiltrating T cells. These results suggest that, in polarized autoreactive effector T cells, miRNA synthesis is inhibited in response to dysregulated RISC assembly, allowing these cells to maintain a highly specific proinflammatory program. Therefore, our findings may provide a mechanism that leads to miRNA dysregulation in EAE/MS.

Key words: **Ago proteins; EAE; miRNA; RISC**

Introduction

Multiple sclerosis is a chronic demyelinating disease of the CNS that manifests a wide spectrum of pathology including inflammation, demyelination, and axonal loss (Moore et al., 1984b). Several immune cell types, immune mediators, and loss of immunoregulatory mechanisms have been implicated in the generation of autoreactive mechanisms in MS (Sospedra and Martin, 2005). Recent studies have suggested a strong association between the dysregulation of different microRNAs (miRNAs) and the development of MS, as well as in the pathogenesis of its animal model, experimental autoimmune encephalomyelitis (EAE; Cox et al., 2010, Junker et al., 2009, 2011; Guerau-de-Arellano et al., 2011; Ponomarev et al., 2011; Mycko et al., 2012; Thamilarasan et al., 2012; Guan et al., 2013; Ode et al., 2012; Ma et al., 2014). miRNAs constitute a class of small, noncoding RNAs that regulate gene expression at the posttranscriptional level, affecting mRNA stability. Although miRNA and other small RNA classes are distinct entities and exert different functions, they all cooperate with members of the Argonaute (Ago) and GW182 families of proteins to form RNA-induced silencing complexes (RISCs) (Kawamata and Tomari, 2010; Kuhn and Joshua-Tor, 2013). RISCs loaded with an miRNA guide strand inhibit mRNAs by two different mechanisms. When the guide strand and target mRNA are fully complementary, the slicer activity of Ago2 cleaves the target mRNA between nucleotides complementary to position 10 and 11 of the guide strands, leading to rapid decay of mRNA (Liu et al., 2004). However, when there is not full complementarity between miRNA and its target sequences, Ago2 recruits GW182 proteins, which are large multidomain proteins, that interact with Ago through their N-terminal glycine and tryptophan-rich (GW) domain (Pauley et al., 2006; Eulalio et al., 2009). The C-terminal part of GW182 contains a bipartite silencing domain that interacts with cytoplasmic polyA-binding protein deadenylases and provides the link between miRNA-target recognition by Ago and mRNA degradation (Liu et al., 2004). Importantly, another partner of RISC, fragile X mental retardation-related protein 1 (FXR1), regulates RISC-

Received Nov. 21, 2014; revised March 18, 2015; accepted March 21, 2015.

Author contributions: P.L. and K.W.S. designed research; P.L., H.C., M.P.M., M.C., M.D., N.L., and A.J. performed research; P.L. analyzed data; P.L., N.L., and K.W.S. wrote the paper.

This work was supported by the National Science Centre (Grant 2014/13/B/NZ6/00235 to P.L., Grant 2013/11/B/NZ6/02055 to H.C., Grant 2011/01/N/NZ6/01849 to M.C., and Grant UMO-2012/04/A/NZ6/00423 to K.W.S.) and the National Center for Research and Development (Grant ERA.NET-RUS/04/2012 to M.P.M.). We thank Celia Brosnan, Albert Einstein College of Medicine (New York, NY) for critical comments and editing of the manuscript.

The authors declare no competing financial interests.

Correspondence should be addressed to Krzysztof W. Selmaj, Department of Neurology, Medical University of Lodz, Ul. Pomorska 251, 92-213 Lodz, Poland. E-mail: kselmaj@afazja.am.lodz.pl.

DOI:10.1523/JNEUROSCI.4794-14.2015

 0270-6474/15/357521-17$15.00/0

dependent posttranscriptional processing by binding with Ago2 (Bhattacharyya and Filipowicz, 2007; Vasudeva and Steitz, 2007; Breving and Esquela-Kerscher, 2010; Fabian et al., 2010). FXR1 is one of the more important FXR family molecules that binds selectively to Ago2 (Vasudeva and Steitz, 2007). In addition, FXR1 has been shown to be involved in posttranscriptional regulation of proinflammatory cytokines such as TNF, IL-1α, IL-1β, IL-6, and GM-CSF through interaction with the ARE located in the 3′-UTR of mRNA (Bhattacharyya and Filipowicz, 2007). Dysregulated RISC assembly also influences miRNA formation and function (Jakymiw et al., 2005; Diederichs and Haber, 2007; Johnston and Hutvanger, 2011; Lund et al., 2011; Winter and Diederichs, 2011). Therefore, miRNA availability and interactions with RISC proteins could contribute to the complexity of posttranscriptional regulatory mechanisms of the immune response (Smibert et al., 2013). Here, we address the role of RISC proteins, in particular the major component Ago2, in the development of EAE. We studied how RISC assembly influences miRNA expression within endogenous CNS cells and in inflammatory infiltrating cells.

Materials and Methods

Subcutaneous immunization with a myelin antigen. C57B/6 mice were housed and maintained in an accredited facility, the Animal Core Department of the Medical University of Lodz. All experiments were approved by University Ethics Committee (12/LB702/2014). Six- to 8-week-old female C57B/6 mice were injected subcutaneously in four abdominal sites with myelin oligodendrocyte (MOG) peptide $MOG_{35–55}$ in CFA. On day 0, each mouse received 0.25 ml of a mixture of 0.15 mg of $MOG_{35–55}$ dissolved in 0.1 ml of PBS containing 0.75 mg of *Mycobacterium tuberculosis* in 0.15 ml of CSF. In addition, 0.2 μg of pertussis toxin (Sigma) was injected into a tail vein on days 0 and 2. Mice were observed daily for neurologic signs of EAE and were scored on the scale from 0 to 5 as follows: 0 = no disease; 1 = weak tail or wobbly walk; 2 = hindlimb paresis; 3 = hindlimb paralysis; 4 = hindlimb and forelimb paralysis; and 5 = death or euthanasia for humane reasons. On day 23, mice were sampled and, after brain reperfusion, brain cells including oligodendrocytes (OLs) were isolated.

Histopathologic examination of CNS. Twenty-three days after injection of MOG or control peptide, representative animals were perfused with 25 ml of cold-buffered 2.5% glutaraldehyde. After brain perfusion, spinal cords were removed, fixed in PFA, and assessed for CNS pathology. An arbitrary inflammation score of 0–4 based on the density of inflammation in the meningeal, perivascular, and parenchymal compartments of the CNS was determined in a blinded fashion according to established criteria (Moore et al., 1984a). A demyelinating score (0–4) was determined according to the number and extent of denuded axons (Moore et al., 1984a).

Isolation of brain-infiltrating T cells, splenocytes, and oligodendrocytes. Under anesthesia, mice were perfused intracardially with PBS and then the brain and spinal cord were removed and homogenized in PBS. Brain mononuclear cells were isolated using 37–70% (v/v) Percoll gradients (Sigma-Aldrich). from mice at the peak (day 23) stage of EAE and sorted by flow cytometry into subsets: T-cell ($TCR\beta^+/CD11b^-$), microglia ($CD11b^+/CD45^{int}$), and macrophages/activated microglia ($CD11b^+/CD45^{high}$). Four or five brains were used for each experiment. To support the conclusion that T cells isolated from EAE brain were mature, effector cells that crossed the blood–brain barrier, we analyzed the expression of cutaneous lymphocyte antigen (CLA), which is a specific indicator for mature lymphocytes that come from the peripheral blood (Piccio et al., 2005). All isolated brain-infiltrating T cells were CLA positive compared with other isolated EAE brain mononuclear cells such as microglia and activated microglia.

Mouse primary OLs were prepared from adult mouse brains and spinal cords. Mice were anesthetized and brains and spinal cords removed. The tissue was cut into small pieces and digested with trypsin (0.25%) and DNase I (0.005%) for 10 min at 37°C. Subsequently, tissue was passed through a mesh and spun down on a continuous Percoll gradient (0–50% Percoll in PBS centrifuged for 30 min 23,500 × *g* in a fixed-angle rotor) for 15 min at 23,500 × *g*. The dissociated cells were suspended in DMEM/F12 (Invitrogen) with 5% FCS supplemented with streptomycin/penicillin, transferrin, insulin, sodium selenite, triiodothyronine, hydrocortisone, biotin, and sodium pyruvate (all Sigma) and then cultured for 2 h in culture flasks. This step enables the separation of adherent cells, such as microglia, from nonadherent cells (OLs; Jurynczyk et al., 2007). The identification and purity of the prepared OLs was determined by immunocytochemical (ICC) staining for myelin associated glycoprotein (MAG) and glial fibrillary acidic protein (GFAP) according to previously established protocols (Jurynczyk et al., 2007; Koenning et el., 2012). $CD3^+$ SCs were isolated using physical disruption of the spleen by passing the tissue through a cell strainer (70 μm; BD Falcon), followed by a negative isolation procedure for $CD3^+$ T cells using magnetic columns (AutoMACS cell sorter; Miltenyi Biotec). To increase the purity of the $CD3^+$ T cells, we used a double-column magnetic separation procedure.

Western blotting. After perfusion, white matter was homogenized in hypotonic buffer (10 mM NaHCO3, 0.2 U/ml aprotynin, 0.5 mM PMSF, pH 7.1, and BSA 1 mg/ml) by Dounce homogenization (all reagents were purchased from Sigma-Aldrich). Lysates were centrifuged (14,000 rpm, 30 min, 4°C) and protein concentration in the lysates was determined using the NanoDrop 2000 spectrophotometer (Thermo Scientific). Total homogenates of samples were resolved on SDS electrophoresis gels by standard procedures. Immunoblotting was performed with rabbit polyclonal anti-GW182 antibody (H-70; Santa Cruz Biotechnology; 1:500 in blocking buffer), rabbit anti-FXR1 antibody (Protein Tech Group, 1:500), rat anti-Ago2 antibody (clone 11A9; Sigma-Aldrich, 1:750), rabbit Ago1 antibody (MBL, 1 μg/ml), goat Ago3 antibody (Santa Cruz Biotechnology, 1:200), and goat Ago4 antibody (Santa Cruz Biotechnology, 1:200). Final detection was achieved with the appropriate secondary antibody coupled to HRP: anti-rabbit IgG-HRP, anti-goat IgG-HRP or anti-rat IgG-HRP (Santa Cruz Biotechnology), followed by Western Lightning ECL Pro substrate (PerkinElmer), and visualized by a gel imaging system for chemiluminescence (G:Box Chemi XR5; Syngene). Equal loading of proteins was checked by immunodetection of β-actin using anti-β actin mouse IgG (Sigma-Aldrich, 1:4000) and anti-mouse IgG-HRP as a secondary antibody (Santa Cruz Biotechnology). The densitometric scanning of the blots and analysis of the visualized bands was performed using a G-Box (Syngene) and Genesys Image Acquisition software, version 1.2.5.0. The results are presented as the intensity of optical density of the area under each band's peak (average value of the pixels enclosed after background correction).

Immunoprecipitation analysis of GW182/Ago2, GW182/FXR1 and Ago2/FXR1. For immunoprecipitation (IP) analysis, fragments of white matter were homogenized in hypotonic buffer as describe above. In parallel, SCs were isolated and lysed in ice-cold RIPA lysis buffer (1% Triton X-100, 20 mM Tris, 150 mM NaCL, pH 7.4) containing 1 mM PMSF, 5 mM NaF, 2 mM activated sodium orthovanadate, 1 mM EGTA, 1 mM EDTA, 1% protease inhibitor mixture for 30 min on ice (all reagents were purchased from Sigma-Aldrich). After centrifugation (14,000 rpm, 30 min, 4°C), the aqueous phase was collected and protein concentration determined using a NanoDrop 2000 Spectrophotometer (Thermo Scientific). Next, primary antibodies against GW182 (mouse mAbs, clone 4B6; Santa Cruz Biotechnology) or Ago2 (rat mAbs, 11A9; Sigma-Aldrich) or pan Ago (clone 2A8; Millipore) were added and incubated with lysates by shaking on ice for 60 min. Twenty microliters of protein A/G PLUS-agarose (Santa Cruz Biotechnology) was added for overnight incubation and rocking on ice. In parallel, the negative control IP was done. The immunoprecipitates were washed 5 times, subjected to SDS PAGE (25 mA, 60 min, room temperature), and immunoblotted for Ago2 or FXR1. After membrane stripping, samples were probed with antibodies to GW182 or Ago2 (analysis of GW182 we used as the positive control IP for Ago2/GW182, FXR1/GW182 complexes and Ago2 we used as the positive control IP for FXR1/Ago2 complexes).

RNA-binding protein immunoprecipitation (RIP). To determine the total miRNA associated with Ago proteins, RNA-binding protein immunoprecipitation (RIP) (Magna RIP; Millipore) was performed according to the manufacturer's protocol and the profile of total miRNA bound to

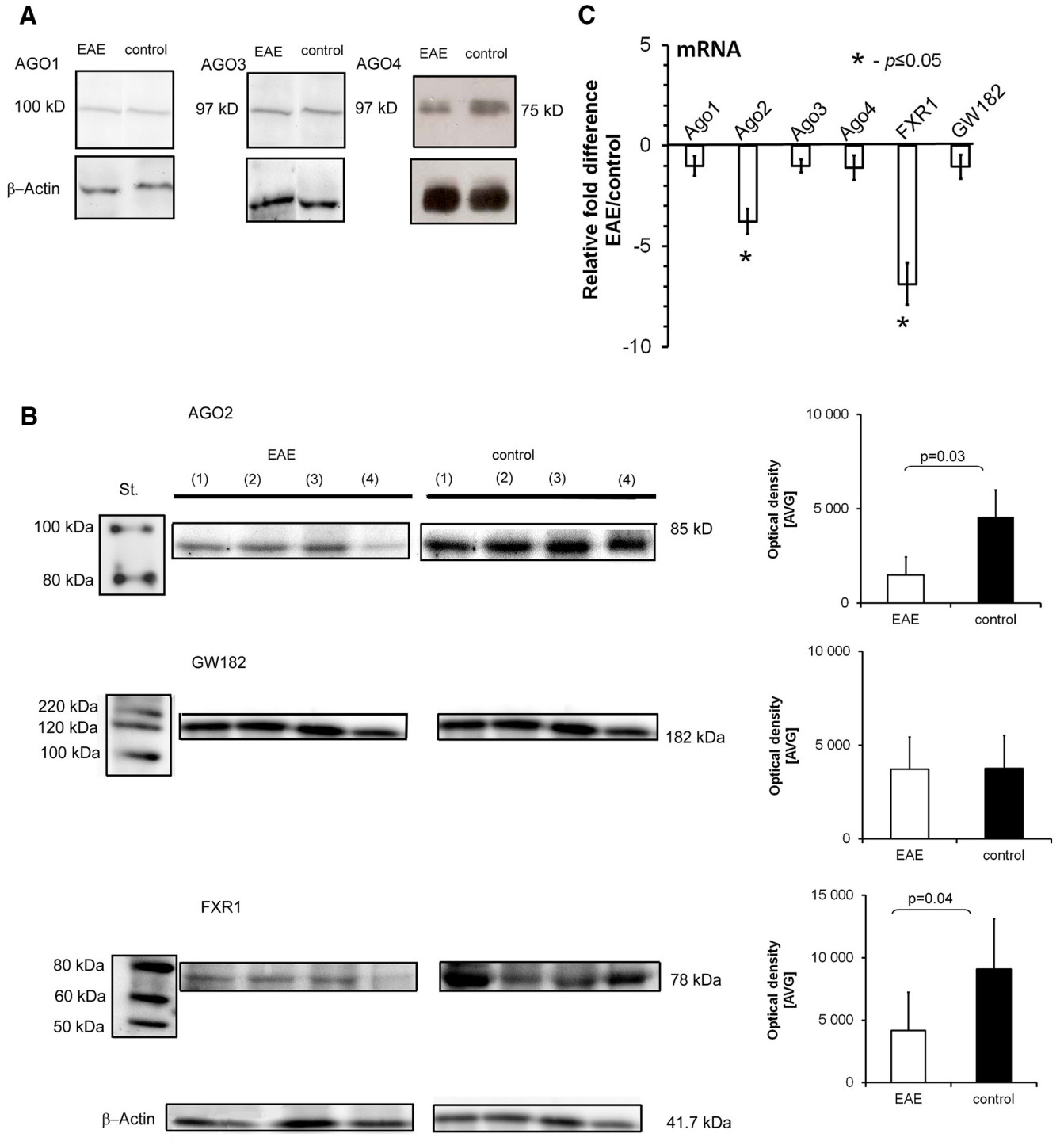

Figure 1. Ago2 and FXR1 downregulation in brain lysates from EAE mice compared with control healthy mice. ***A***, Examples of Western blot analysis for Ago1, Ago3, and Ago4. ***B***, Western blot analysis for Ago2, GW 182, and FXR1 in whole-brain protein lysates. Each value represents data for brain lysates isolated from four EAE and four control mice. Histograms show average optical density ± SD. ***C***, mRNA expression in whole-brain lysates. Data represent the mean of relative mRNA expression (EAE/control) ± SD from four independent experiments (five mice per experiment).

Ago was checked with a 2100 Bioanalyzer System and a small RNA kit (Agilent Technologies)

Immunohistochemistry. For immunohistochemistry (IHC), after whole mouse perfusion with paraformaldehyde, the brain and spinal cord were prepared and frozen in sectioning medium (−80°C, Neg50; Richard-Allan Scientific). The brain was cut into 6 μm sections at −20°C using cryostat microtome method (MTE-S; Slee) and transferred to gelatin-coated microscope slides. Samples were fixed with ice-cold acetone (10 min) and washed three times in PBS. Subsequently, slides were blocked (10% normal blocking serum in PBS, supplemented with 0.3% Triton X-100. and 0.01% sodium azide; 20 min at room temperature) and washed. Sera were derived from the same species as secondary mAbs (Santa Cruz Biotechnology). Samples were incubated overnight with an appropriate first antibody (Ago2, GW182, FXR1, MAG), washed, and subsequently stained with the appropriate secondary fluorescent antibodies supplemented with 1.5% normal blocking rabbit serum and 0.3% Triton X-100; 0.01% sodium azide was added for 1 h at 21°C (goat pAb to rabbit Cy3, goat pAbs to mouse FITC; Abcam, 1:100). For fluorescent

DNA nuclei staining, DAPI (1.5 μg/ml UltraCruz Mounting Medium; Santa Cruz Biotechnology) was used. Images were acquired using a confocal microscope (BD Biosciences PathwayTM Bioimager 850 with AttoVision 1.5.3 software). For quantitative fluorescence intensity analysis, an Olympus UApo/340 20× 0.75 objective was used and microscope slides were analyzed by IPLab Pathway 4.0 software (BD Biosciences). The final image was prepared from a montage of at least 250 single images. Fluorescence intensity is expressed as the average fluorescence of the measured segments (sum of the fluorescence regions of all segments divided by the number of segments) and total intensity (total area; Dima et al., 2011).

ICC analysis. For quantitative immunofluorescence analysis, isolated cells were transferred to gelatin-coated microscope slides by cytospin (300 × *g*, 10 min) and fixed with PBS containing 4% (w/v) paraformaldehyde for 20 min at 21°C. Fixed cells were washed extensively with PBS and blocked with 10% rabbit normal blocking serum (Santa Cruz Biotechnology) supplemented with 3% Triton X-100 (Sigma-Aldrich) for 45 min at 21°C. Next, cells were washed and incubated with unlabeled 5 μg/ml anti-mouse Ago2 with FXR1, Ago2 with GW182, anti-GFAP (rabbit polyclonal antibody; Santa Cruz Biotechnology 1:300), or anti-MAG (goat polyclonal; Santa Cruz Biotechnology, 1:300). As negative isotype controls, we used rat IgG2b (Invitrogen). All antibodies were suspended in the PBS supplemented with 1.5% normal blocking rabbit serum, 0.3% Triton X-100, and 0.01% sodium azide and incubated for 1 h at room temperature in a wet chamber. Subsequently, cells were washed in PBS 3 times and the appropriate secondary fluorescent antibody supplemented with 1.5% of normal blocking rabbit serum and 0.3% Triton X-100 and 0.01% sodium azide were added for 1 h at 21°C (rabbit preadsorbed polyclonal TRITC to rat; Abcam; goat pAb to rabbit Cy3 or goat pAbs to mouse FITC; Abcam). For fluorescent DNA nuclei staining, DAPI (1.5 μg/ml UltraCruz Mounting Medium; Santa Cruz Biotechnology) was used. Images were acquired using spin confocal microscope BD Biosciences PathwayTM Bioimager 850 with AttoVision 1.5.3 software. For quantitation of the fluorescence intensity analysis, an Olympus PlanApo N 60×1 oil objective was used and 16 sites per microscope slides were analyzed by IPLab Pathway 4.0 software (BD Bioscience). Fluorescence intensity was determined as the average fluorescence (average area), the the sum of the fluorescence from all segments divided by the number of segments (Dima et al., 2011). The average fluorescence was calculated using at least 100 single cells taken from four independent experiments.

RNA isolation and real-time PCR. Total RNA was isolated from brain tissue using TRIzol (Invitrogen) and the RNeasy Mini Kit (Qiagen) according to the manufacturer's instructions and treated with RNase-free DNase I (Qiagen) to remove contaminating genomic DNA. One microgram of the total RNA was reverse transcribed to cDNA with random hexamers and M-MMLV reverse transcriptase using ReactionReadyTM First Strand cDNA Synthesis Kit (SuperArray Bioscience Corporation). Primer sequences were as follows: Ago2 reverse primer, 5′-TTA CCA TCC ATG AGG TAC ACC CCT G-3′; GW182: 5′-AGC AAA CAT GGT GCT ATT TCA AGT G-3′; Ago1: 5′-AGT CAA CCG GGA GGT GGT GGA ATA C-5′; AGO3: 5′-AGA AAG GGT TGG AAG AAG CGG CAA C-3′; Ago4: 5′-TAG AGT CAA CAG GGA GGT GGT AGA C-3′; Ago5: 5′-ATC CAC AAc GTG GGC TAG TCC G-3′; FXR1: 5′- TTG AAA ATA ATTGGC AAC CAG AAC G-3′; β-actin: 5′-TGT TAC TGA GCT GCG TTT TAC ACC C-3′. cDNA was amplified in the presence of specific primers in 96-well microtiter plates on a 7500 Real Time PCR System (Applied Biosystems) according to the following program: 95°C for 10 min and 40 cycles of 95°C for 15 s and 60°C for 60 s. Separate samples from EAE and controls were measured in triplicate. As a positive control, cDNA synthesized from mouse XpressRefTM Universal Reference Total RNA was used (SuperArray Bioscience). Specificity of the reaction was checked by melting curve analysis, and relative expression of the genes was determined using a software program supplied by Applied Biosystems. All of the reagents, TaqMan Gene Expression Master Mix, 20× TaqMan gene expression Assay Mix, and specific primers were provided by Applied Biosystems.

miRNA isolation and analysis. miRNA was isolated from brain tissue, isolated OLs, splenocytes, and EAE brain-infiltrating T cells using an acid-phenol:chloroform procedure and a mirVana miRNA isolation kit (Ambion) according to the manufacturer's instructions. After isolation, the level of miRNA and the purity analysis was performed by a commercially available small RNA kit (2100 Bioanalyzer; Agilent Technologies 2100 expert software). For each sample, the level of miRNA was normal-

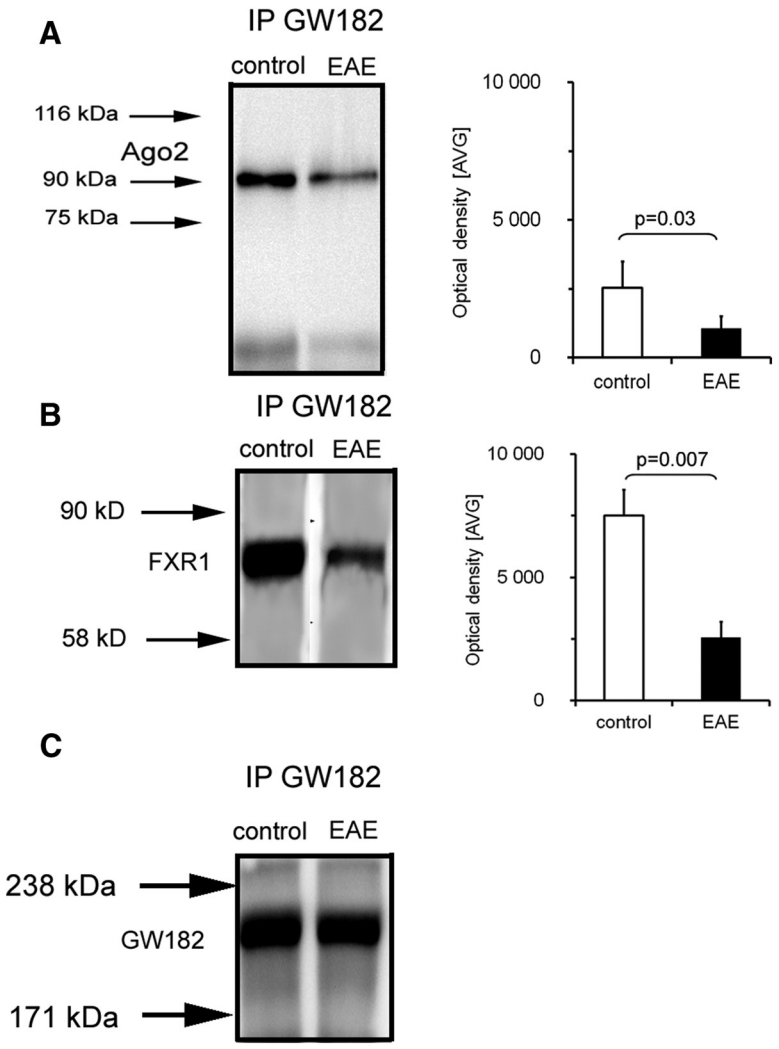

Figure 2. Coimmunoprecipitation of Ago2 and FXR1 with GW182 in brain lysates of EAE and control healthy mice. ***A***, Decreased Ago2 coexpression in GW182 complex in the EAE brain compared with control mice. ***B***, Decreased FXR1 coexpression in GW182 complex in the brain in EAE compared with control mice. Ago2 and FXR1 were normalized to GW182. ***C***, Expression of GW182 in control and EAE brain tissue. Histograms depict optical density of the area under each band's peak ± SD taken from four independent experiments (four mice per experiment).

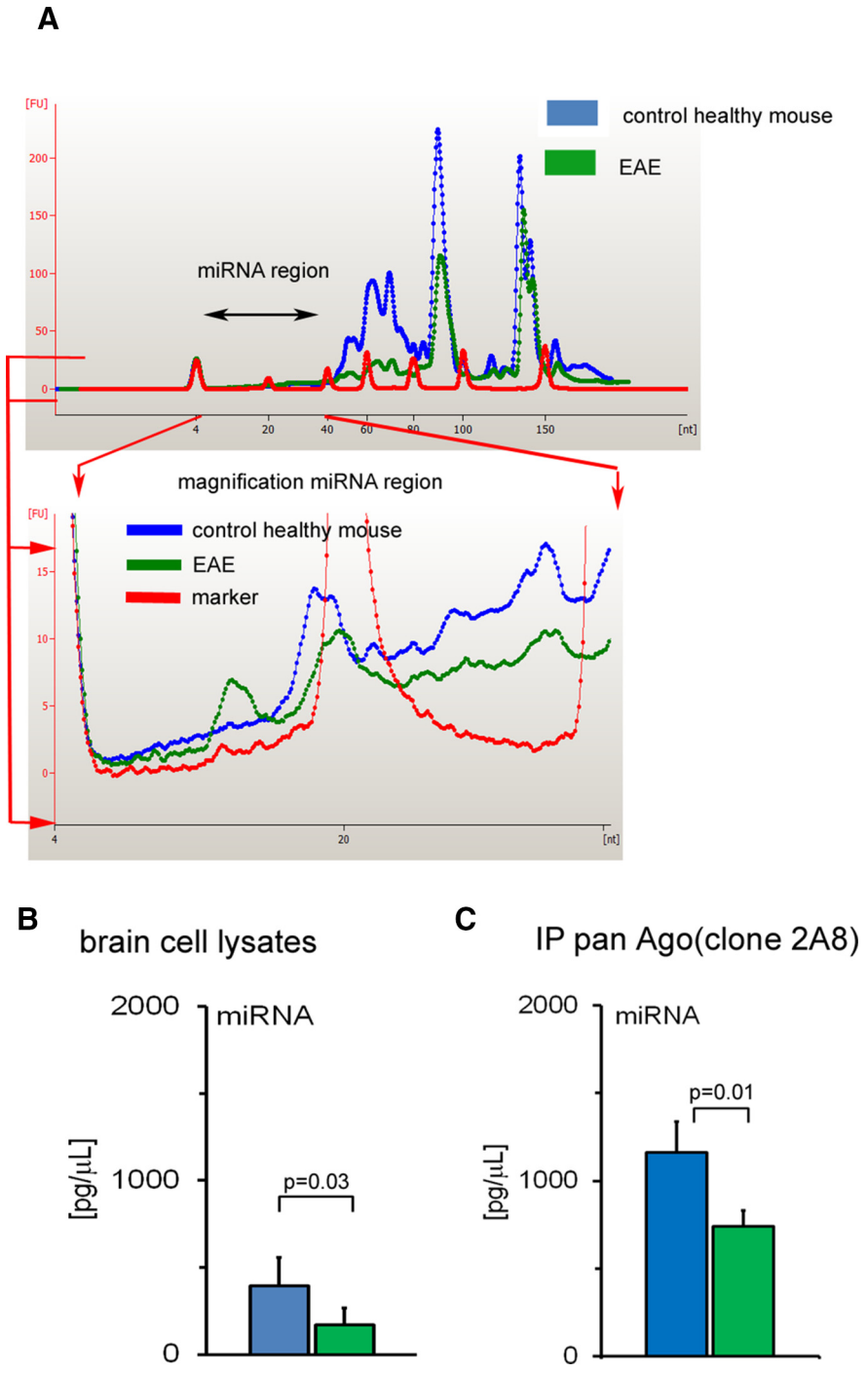

Figure 3. Downregulation of miRNAs in EAE whole-brain lysates. ***A***, miRNA-containing region (magnified at bottom) was defined arbitrarily ranging from 10 to 40 nt. Data are presented as the mean of miRNA concentration ± SD from four experiments. miRNA was normalized to total mRNA levels. ***B***, Diminished global miRNA expression in EAE brain. ***C***, Diminished global miRNA expression in coimmunoprecipitates with Ago proteins (pan Ago). The bars represent a mean expression ± SD from four independent experiments (four mice per experiment).

ized to total RNA quantified using Agilent Technologies RNA Pico Chips (2100 Bioanalyzer).

Multiple miRNA profiling microarray (miRNA real-time qRT-PCR). Specific miRNA expression was analyzed using mice miScript miRNA PCR Array (Qiagen). cDNA was amplified in the presence of 84 specific primers (NCBI accession numbers and gene symbols are presented in Tables 1 and 2), coated in 96-well microtiter plates on a 7500 Real Time PCR System (Applied Biosystems) according to the following program: 95°C for 15 min (activation of HotStarTaq DNA polymerase); 40 cycles of 94°C for 15 s, 55°C for 30 s, and 70°C for 30 s. The mean expression levels of the six snoRNA/snRNA panels (SNORD6, SNORD68, SNORD72, SNORD95, SNORD96A, and RNU6-2) were used for normalization of the data.

Statistical analysis of mRNA and miRNA expression. Data from real-time PCR were calculated using the ΔΔCt method as described previously (Hansel et al., 2008). The complete calculation was as follows:

$$\frac{\frac{2^{-Ct(GOI)}EAE}{2^{-Ct(HKG;snoRNA/snRNA)}EAE}}{\frac{2^{-Ct(GOI)}h.m.}{2^{-Ct(HKG;snoRNA/snRNA)}h.m.}} = \frac{2^{-[Ct(GOI)-Ct(HKG;snoRNA/snRNA)]}EAE}{2^{-[Ct(GOI)-Ct(HKG;snoRNA/snRNA)]}h.m.} = \frac{2^{\Delta Ct}EAE}{2^{\Delta Ct}h.m.} = 2^{\Delta\Delta Ct}$$

Where GOI is the gene of interest (mRNA or miRNA factors); HKG is the housekeeping genes or snoRNA/snRNA control for miRNA normalization; Ct is the threshold cycle; ΔΔCt is equal to ΔCt (EAE) − ΔCt (h.m.); and h.m. is healthy mice.

Statistics. Arithmetic means and SDs were calculated for all parameters in at least four independent experiments. For WB, IP, qPCR, and IHC methods, EAE and control groups contained four mice each. For IP, ICC, and miRNA analysis performed on isolated brain mononuclear cells, $CD3^+$ SCs and OLs, six mice from each group were taken for a single experiment and four independent experiments were performed. A statistical analysis of differences was performed using the one-way ANOVA test. Scheffe's test was used for multiple comparisons as a *post hoc* test when statistical significances were identified in the ANOVA test. Statistical significance was set at $p < 0.05$.

Results

RISC proteins in EAE brain

We analyzed the composition of RISCs in brain tissue by measuring the expression of Ago1, Ago2, Ago3, Ago4, GW182, and FXR1 in EAE and healthy mice by Western blot and q-mRNA. The data showed that, whereas the levels of Ago1, Ago3, and Ago4 and GW182 were not altered in EAE mice, Ago2 and FXR1 were downregulated in EAE brain tissue at both the protein and mRNA level (Fig. 1). Densitometric analysis of Western blots gave values for Ago2 in EAE of 1503 ± 942 versus control 4557 ± 1440; FXR1 in EAE 4190 ± 3030 versus control 9080 ± 4031; and GW182 in EAE 3725 ± 1692 verseus control 3750 ± 1758 AVG (Fig. 1*A*,*B*). qPCR analysis showed decrease relative fold differences in EAE to control group by3.8 ± 0.63 for Ago2; by 6.9 ± 1.03 for FXR. For GW182, the fold difference was not significant (−0.9 ± 0.68) between EAE and control (Fig. 1*C*). To confirm that Ago2 was decreased in RISCs, we assessed the

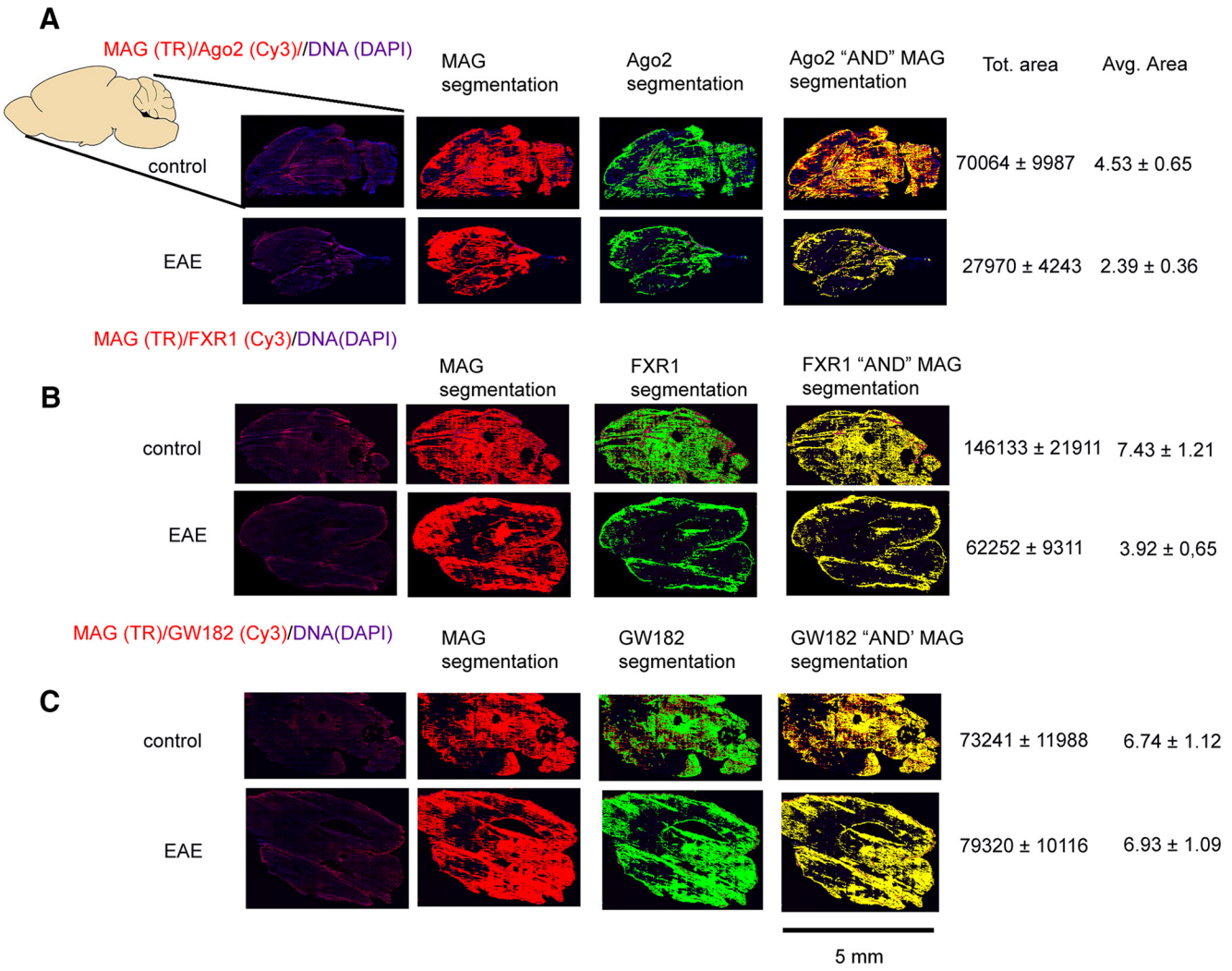

Figure 4. Whole-brain IHC analysis of Ago2, FXR1, and GW182 in EAE compared with control healthy mice. ***A***, Ago2 expression was decreased in EAE brain (green) and in MAG-positive cells versus healthy mice brain (yellow in merge images). ***B***, FXR1 expression was decreased in EAE brain (green color) and in MAG-positive cells (yellow color) versus healthy mice brain. ***C***, Expression of GW182 was not different in EAE versus healthy mice in whole-brain and in MAG-positive cells. Frozen 6 μm sagittal cross-sections of whole brain were prepared, scanned, and the final image prepared from a montage of at least 250 single images. Average fluorescence (average area) and total fluorescence intensity (Tot. Area) were analyzed using an electronic fluorescence autosegmentation system (BD Biosciences AttoVision software). The isotype control and secondary antibody incubated without the first Ab were negative.

amount of Ago2 in complexes with GW182 and FXR1 in brain lysates by immunoprecipitation. The data showed less intense signal for Ago2 (1193 ± 476 vs control 2509 ± 981 AVG) and FXR1 (2497 ± 1087 vs control 7598 ± 1201 AVG) in complexes with GW182 in EAE (Fig. 2*A*,*B*). These results indicate an altered composition of RISCs in the brain tissue of mice with EAE.

Dysregulation of global miRNA levels in EAE brain

Previous studies have suggested that dysregulation and/or deactivation of RISC proteins during inflammation might affect total miRNA levels (Jakymiw et al., 2005; Liu et al., 2005; Pillai et al., 2005; Boudreau et al., 2014). To test whether this mechanism might operate in EAE, we then analyzed the total level of small RNAs (up to 150 nt), including miRNA (up to 40 nt), in whole brain cell lysates of EAE and control mice (Fig. 3*A*). We found that total miRNA levels were decreased (171 ± 97 pg/μl) at the peak of disease compared with healthy control mice (396 ± 162 pg/μl; Fig. 3*B*). Subsequently, we analyzed the total amount of miRNAs associated with RISC proteins. Ago proteins were immunoprecipitated and miRNA levels measured as described in Material and Methods. This analysis showed that the amount of miRNA bound to Ago proteins was diminished by 1/3 in EAE mouse brain tissue compared with levels found in healthy mice (740 ± 118 vs 1162 ± 179 pg/μl; Fig. 3*C*). Therefore, these results support the hypothesis that dysfunction of RISC assembly correlates with decreased total amounts of miRNAs in whole EAE brain tissue.

Ago2 and FXR1 are downregulated within RISC in OLs during EAE

To address the RISC composition in CNS target cells affected by immune attack in EAE/MS, we first measured RISC protein expression in OLs by IHC using a double-staining procedure. The IHC analysis demonstrated that Ago2 and FXR1 expression measured as the total area values were downregulated in OLs in EAE (Ago2 in EAE 27,970 ± 4243 vs control 70,064 ± 9987; FXR1 in EAE 62,252 ± 9311 vs control 146,133 ± 21,911), whereas the expression of GW182 did not differ from that found in healthy mice (79,320 ± 10,116 vs 73,241 ± 11,988; Fig. 4). Analysis of the average area values confirmed decreased Ago2 (2.39 ± 0.36) and

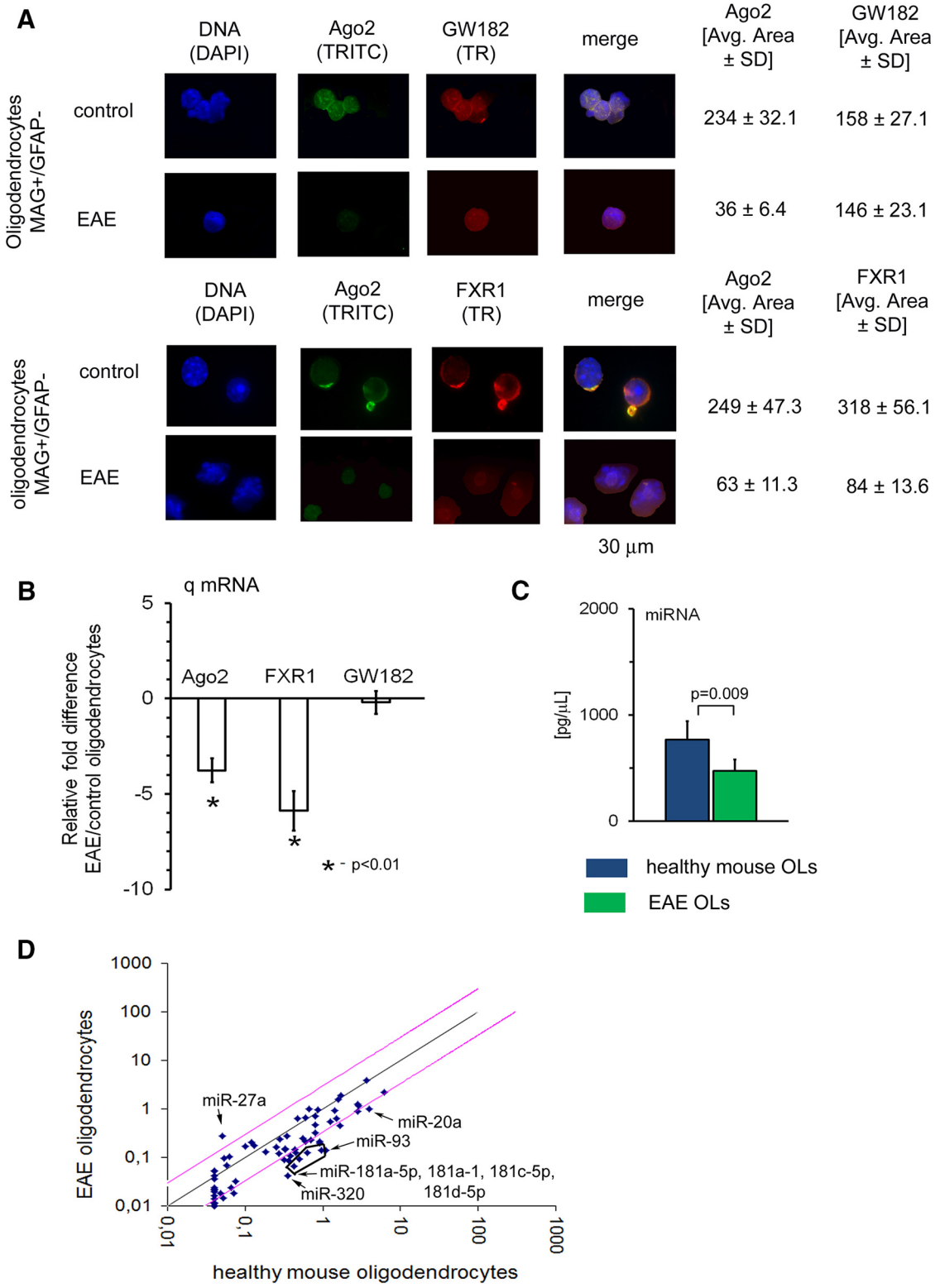

Figure 5. Decreased expression of Ago2 and FXR1 and the deficient formation of Ago2/GW182 and Ago2/FXR1 complexes in EAE OLs. ***A***, ICC analysis of Ago2/GW182 (top) and Ago2/FXR1 (bottom) in *ex vivo* isolated OLs. Yellow areas on the merged images indicate colocalization of Ago2 with GW182 and Ago2 with FXR1. The isotype control and secondary antibody incubated without the first Ab were negative. Numerical data from four independent experiments are presented as a sum of the fluorescence regions of all segments divided by the number of segments (average area). ***B***, mRNA for Ago2, GW182, and FXR1 relative expression in EAE compared with healthy OL lysates. Data represent the mean of relative mRNA expression ± SD from four independent experiments. ***C***, Diminished global miRNA levels in EAE compared with healthy OLs. The bars represent the mean amount of miRNA from four independent experiments (four mice per experiment). ***D***, Differential expression of 86 miRNAs in EAE OLs versus OLs isolated from healthy mice. The pink lines indicate thresholds of at least 3-fold upregulation or downregulation of respective miRNA levels. Data are representative of three independent experiments.

Table 1. Fold differences in relative miRNA expression between EAE and healthy mice OLs

miRNA	NCBI accession no.	Fold change EAE OLs/healthy OLs
let-7b-5p	MIMAT0000522	−2.16
let-7c-5p	MIMAT0000523	−2.25
let-7d-5p	MIMAT0000383	−2.33
let-7e-5p	MIMAT0000524	−1.83
let-7i-5p	MIMAT0000122	−3.11
miR-101a-3p	MIMAT0000133	−3.66
miR-101b-3p	MIMAT0000616	−3.63
miR-105	MIMAT0004856	−3.94
miR-106b-5p	MIMAT0000386	−4.56
miR-107-3p	MIMAT0000647	−3.46
miR-124-3p	MIMAT0000134	−2.49
miR-125b-5p	MIMAT0000136	−1.69
miR-126a-5p	MIMAT0000137	−2.00
miR-128-3p	MIMAT0000140	1.32
miR-133b-3p	MIMAT0000769	−3.94
miR-134-5p	MIMAT0000146	−3.94
miR-135b-5p	MIMAT0000612	−3.94
miR-138-5p	MIMAT0000150	1.62
miR-139-5p	MIMAT0000656	−1.69
miR-140-5p	MIMAT0000151	−2.32
miR-146a-5p	MIMAT0000158	1.72
miR-146b-5p	MIMAT0003475	1.29
miR-148b-3p	MIMAT0000580	−1.11
miR-151-3p	MIMAT0000161	−3.92
miR-152-3p	MIMAT0000162	−1.90
miR-15a-5p	MIMAT0000526	−4.98
miR-15b-5p	MIMAT0000124	−4.01
miR-181a-5p	MIMAT0000210	−5.51
miR-181a-1-3p	MIMAT0000660	−3.94
miR-181c-5p	MIMAT0000674	−6.42
miR-181d-5p	MIMAT0004324	−6.83
miR-191-5p	MIMAT0000221	−1.54
miR-193b-3p	MIMAT0004859	−3.94
miR-194-5p	MIMAT0000224	−2.43
miR-195a-5p	MIMAT0000225	−2.72
miR-19b-3p	MIMAT0000513	−2.23
miR-203-3p	MIMAT0000236	−3.60
miR-20a-5p[a]	MIMAT0000529	−3.70
miR-20b-5p	MIMAT0003187	−4.30
miR-22-3p	MIMAT0000531	−2.27
miR-24-3p	MIMAT0000219	−1.01
miR-26b-5p	MIMAT0000534	−1.26
miR-27a-3p[b]	MIMAT0000537	5.27
miR-28a-5p	MIMAT0000653	1.05
miR-298-5p	MIMAT0000376	−3.94
miR-29a-3p	MIMAT0000535	−1.15
miR-29b-3p	MIMAT0000127	1.78
miR-29c-3p	MIMAT0000536	−2.21
miR-30a-5p	MIMAT0000128	−2.46
miR-30d-5p	MIMAT0000515	1.10
miR-30e-5p	MIMAT0000248	−3.14
miR-320-3p	MIMAT0000666	−8.38
miR-328-3p	MIMAT0000565	−4.23
miR-33-5p	MIMAT0000667	−3.94
miR-337-3p	MIMAT0000578	−3.94
miR-338-3p[b]	MIMAT0000582	−9.94
miR-339-5p	MIMAT0000584	1.32
miR-342-3p	MIMAT0000590	1.18
miR-346-5p	MIMAT0000597	−3.94
miR-34a-5p	MIMAT0000542	−1.57
miR-376b-3p	MIMAT0001092	−3.58
miR-381-3p	MIMAT0000746	−3.94
miR-409-3p	MIMAT0001090	−3.94
miR-431-5p	MIMAT0001418	−3.94
miR-433-3p	MIMAT0001420	−2.67
miR-455-5p	MIMAT0003485	−3.94
miR-484	MIMAT0003127	−2.80
miR-485-5p	MIMAT0003128	−3.94
miR-485-3p	MIMAT0003129	−3.94
miR-488-3p	MIMAT0003450	−3.94
miR-489-3p	MIMAT0003112	−3.94
miR-598-3p	MIMAT0004942	−2.77
miR-652-3p	MIMAT0003711	−1.17
miR-7a-5p	MIMAT0000677	1.66
miR-9-5p	MIMAT0000142	−1.40
miR-9-3p	MIMAT0000143	−3.61
miR-92a-3p[a]	MIMAT0000539	−2.30
miR-93-5p	MIMAT0000540	−7.76
miR-98-5p	MIMAT0000545	−3.94

[a]miRNAs associated with myelin protein synthesis and survival OLs.

[b]miRNAs associated with differentiation and proliferation of OLs.

FXR1 (3.92 ± 0.65) expression versus control 4.53 ± 0.65 and 7.43 ± 1.21 for Ago2 and FXR1, respectively. GW182 expression was not changed in EAE 6.93 ± 1.09 versus control 6.74 ± 1.12 (Fig. 4).

Next, we examined RISC protein expression in OLs isolated from EAE brain tissue. The ICC analysis confirmed that both Ago2 and FXR1 proteins were decreased in OLs from EAE brain samples compared with control mouse brains (Ago2 in EAE 36 ± 6.2 vs control 234 ± 32.1; FXR1 in EAE 63 ± 11.3 vs control 249 ± 47.3 average area; Fig. 5*A*). The expression of GW182 was unchanged in OLs from EAE brain (EAE 146 ± 23.1 vs control 158 ± 27.1 average area; Fig. 5*A*). In addition, we found that signal for Ago2 in double-stained OLs, Ago2/GW182 and Ago2/FXR1, from EAE mouse brains showed lower expression compared with OLs from control healthy mouse brains (Fig. 5*A*). These findings suggest the deficient presence of Ago2 in RISC of OLs during EAE. This was confirmed by measurements of mRNA expression for Ago2, FXR1, and GW182 in OLs (Fig. 5*B*). The relative fold differences in EAE compared with control showed decreased by 3.9 ± 0.76 for Ago2 and by 6.3 ± 1.16 for FXR1. mRNA for GW182 in EAE was not different from control OLs (fold difference −0.2 ± 0.53 for GW182; Fig. 5*B*).

Dysregulation of miRNAs in EAE OLs

Inadequate composition of RISCs in OLs might affect miRNA machinery. We investigated the global level of miRNAs in OLs from EAE and control brain tissue. Freshly *ex vivo* isolated OLs were used for RNA isolation. Total RNA was measured and used for normalization of miRNA expression. Compared with total RNA, global miRNA expression was downregulated in OLs derived from brain tissue of EAE animals harvested at the peak of disease (EAE 474 ± 109.0 vs control 767 ± 176.4 pg/μl; Fig. 5*C*). Next, we analyzed a panel of 86 miRNAs previously found to be associated with OL cell survival within the CNS using real-time qRT-PCR (Table 1). As shown in Figure 5*D*, levels of the majority of miRNAs were decreased in OLs from EAE brain tissue compared with OLs from control healthy mice. Fifty-six CNS-related miRNAs of 86 examined were downregulated (fold change < −2.0), 22 miRNAs were unchanged (range −1.9–1.9), and miR-27a-3p was upregulated (fold change 5.4). The most strikingly downregulated miRNAs, 106b-5p, 15a-5p, 15b-5p, 181a-5p, 181c-5p, 181d-5p, 20b-5p, 320-3p, 328-3p, and 338-3p, have been found previously to be linked to differentiation, prolifera-

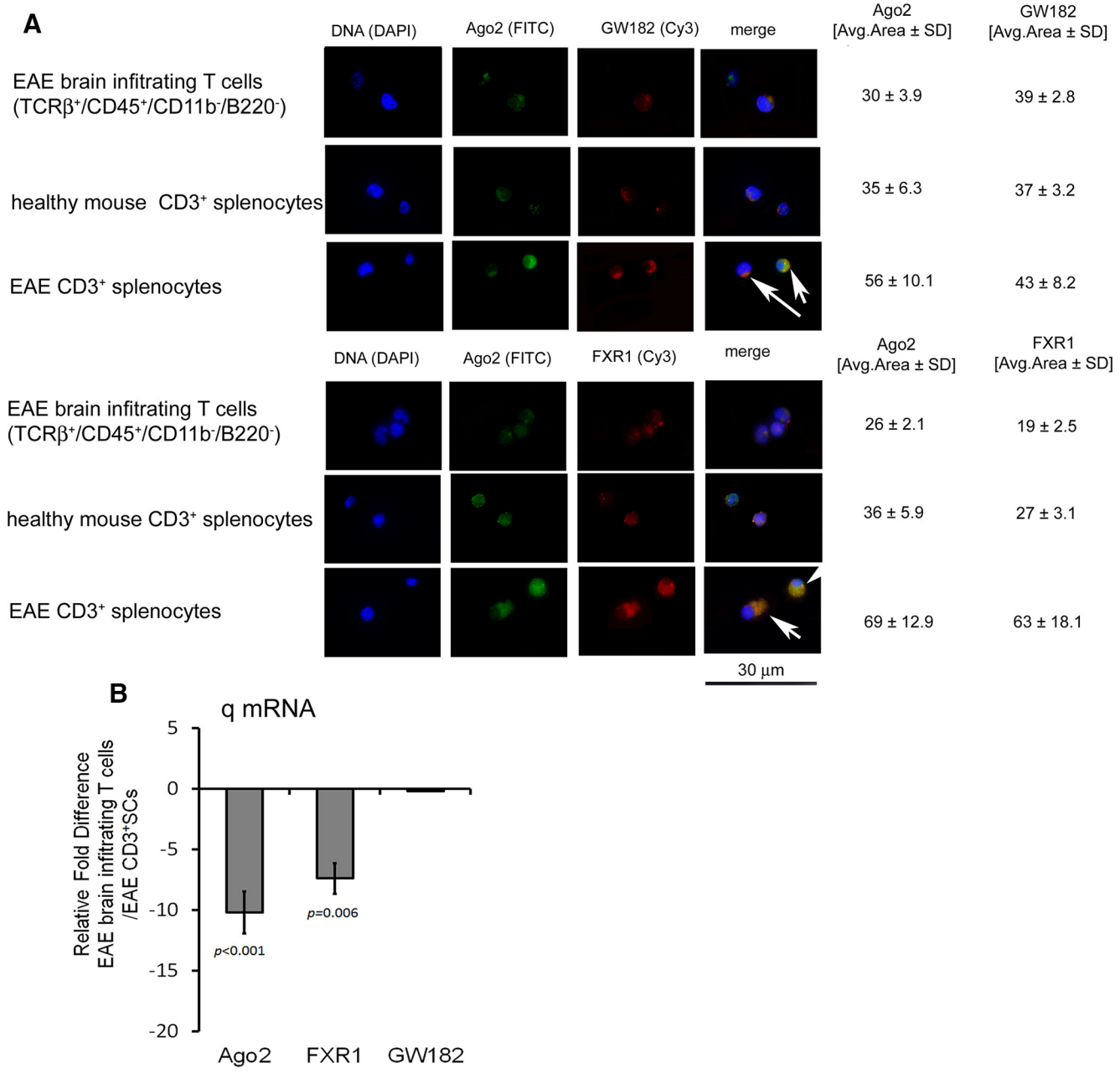

Figure 6. Decreased expression of Ago2 and FXR1 in brain-infiltrating T lymphocytes in EAE and deficiency formation of Ago2/GW182 and Ago2/FXR1 complexes. ***A***, ICC analysis of Ago2/GW182 (top) and Ago2/FXR1 (bottom) proteins in EAE brain-infiltrating T cells and CD3 $^{+}$ SCs from EAE and healthy mice. Yellow areas on merged images (arrows) indicate colocalization of Ago2 with GW182 and Ago2 with FXR1. The isotype control and secondary antibody incubated without the first Ab were negative. Numerical data from four independent experiments are presented as a sum of the fluorescence regions of all segments divided by the number of segments (average area). ***B***, mRNA for Ago2, FXR1, and GW182 expression in EAE brain-infiltrating T cells compared with EAE CD3 $^{+}$ SCs. Data represent the mean of relative mRNA expression ± SD from four independent experiments (four mice per experiment).

tion, and myelin protein synthesis (Fig. 5*D*, Table 1; Zheng et al., 2012). Most importantly, we found that the miRNA-17-92 cluster represented by miRNA-20a and miRNA-92a-1 was specifically downregulated in OLs during EAE. Recent studies have shown that this miR-17-92 cluster is essential for the differentiation, proliferation, and survival of OLs (Budde et al., 2010). Another striking observation was that miRNA-338-3p was the most extensively decreased miRNA (nearly 10-fold) in EAE OLs compared with healthy OLs; this miRNA, together with miR-338-5p, has been implicated in the regulation of oligodendrocyte precursor cell (OPC) differentiation and myelin gene expression (Dugas et al., 2010; Wang and Cambi, 2012; de Faria et al., 2012). The only upregulated miRNA in EAE OLs found in our study was miR-27a-3p, which has been linked to the control of cell proliferation (Lerner et al., 2011; Xu et al., 2013).

Ago2 and FXR1 were downregulated within RISC in infiltrating T cells from EAE brain

To address RISC composition in EAE brain-infiltrating T cells, we isolated T cells from CNS tissue of EAE mice and measured Ago2, GW182, and FXR1 expression and compared them with levels found in splenocytes from the same animals. The data showed that Ago2 and FXR1 were downregulated in infiltrating T cells compared with SCs from EAE animals (Ago2 30 ± 3.9 vs

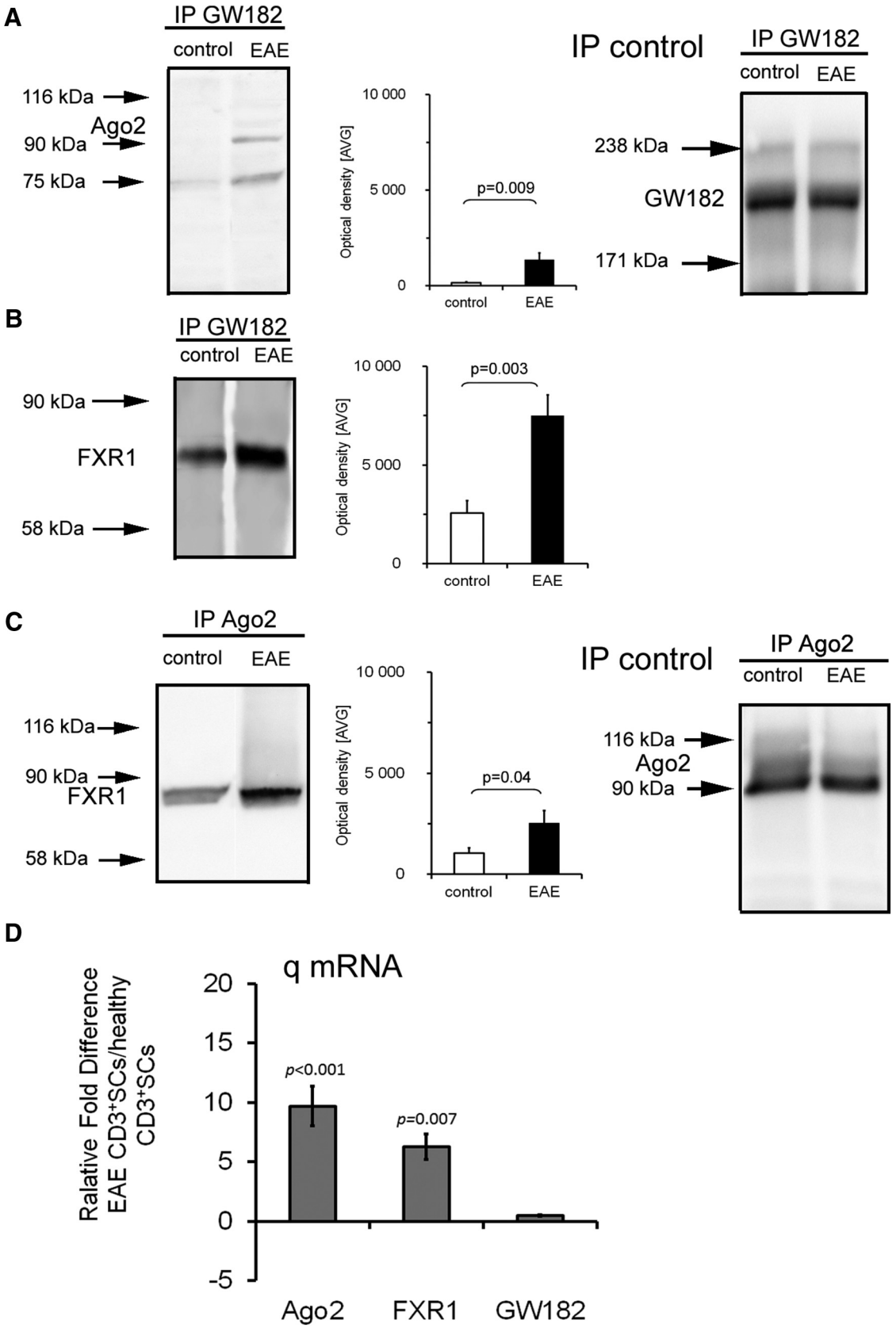

Figure 7. Coimmunoprecipitation of Ago2, GW182, and FXR1 in CD3 $^{+}$ SCs of EAE and control healthy mice. ***A***, Increased Ago2 expression in Ago2/GW182 complexes. ***B***, Increased FXR1 expression in FXR1/GW182 complexes. ***C***, Increased FXR1 expression in FXR1/Ago2 complexes in EAE CD3 $^{+}$ SCs versus control CD3 $^{+}$ SCs. Ago2 and FXR1 Western blots were normalized to GW182 (right top) and for FXR1/Ago2 immunoprecipitation to Ago2 (right bottom). Data are presented as the intensity of optical density of the area under each band's peak $\pm$ SD. Each bar represents mean data from four independent experiments (four mice per experiment). ***D***, mRNA for Ago2, FXR1, and GW182 in EAE CD3 $^{+}$ SCs compared with control healthy mouse CD3 $^{+}$ SCs. Data represent the mean of relative mRNA expression $\pm$ SD from four independent experiments (four mice per experiment).

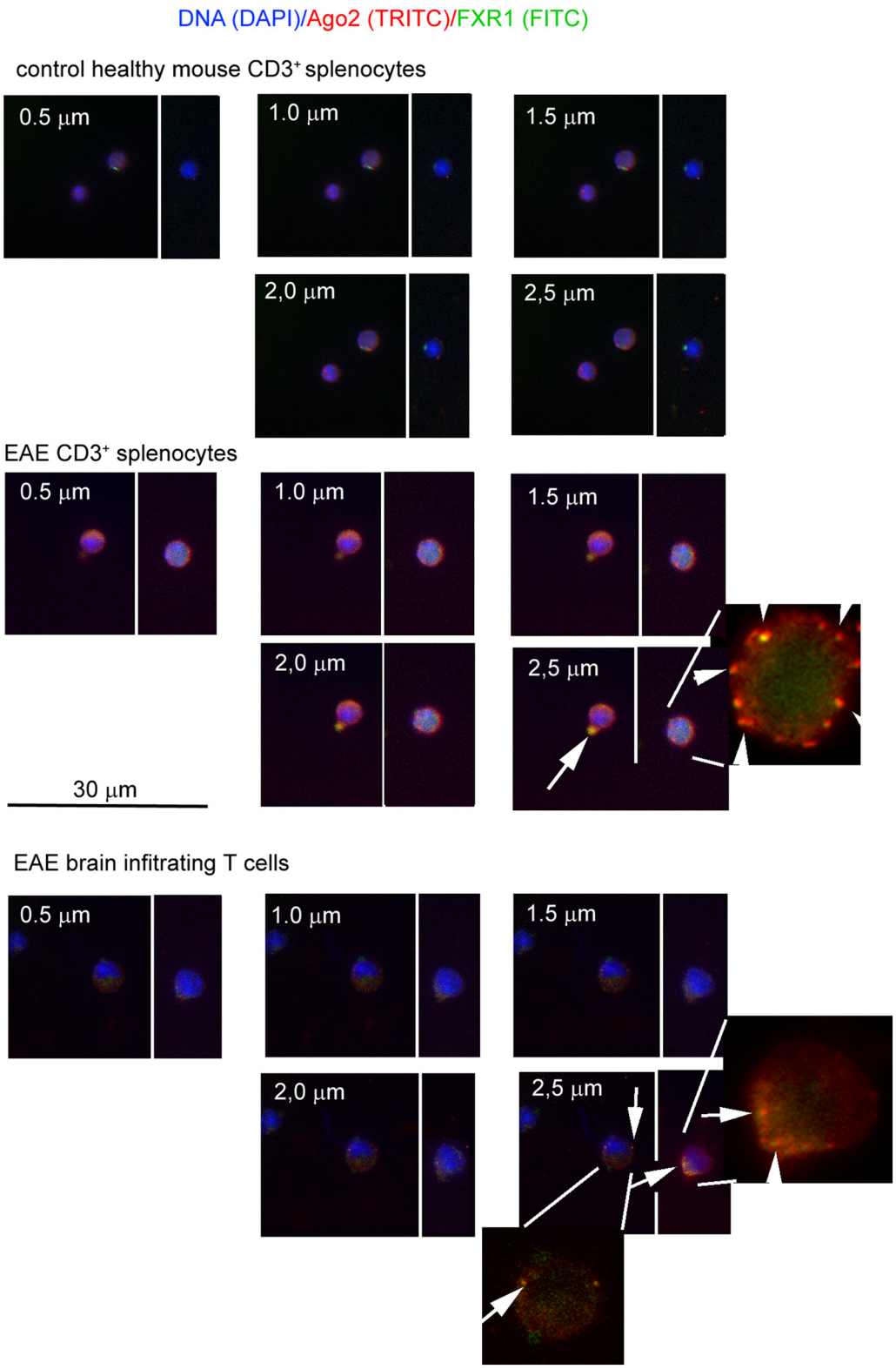

Figure 8. Confocal microscopy analysis of FXR1 with Ago2 in EAE CD3 $^{+}$ SCs and EAE brain-infiltrating T lymphocytes compared with CD3 $^{+}$ SCs from healthy mice. Arrows highlight more intense formation of Ago2/FXR1 complexes (yellow color) in EAE CD3 $^{+}$ SCs compared with healthy CD3 $^{+}$ SCs or brain-infiltrating T cells. To better visualize colocalization of FXR1 with Ago2, three representative merged cells without DNA signal were magnified.

56 ± 10.1 average area; FXR1 19 ± 2.5 vs 63 ± 18.1 average area) and also compared with SCs from control mice (Ago2 35 ± 6.3 average area; FXR1 27 ± 3.1 average area; Fig. 6*A*). GW182 expression remained at the same level in EAE as in control mice (EAE brain-infiltrating T cells 39 ± 2.8 vs EAE CD3 $^{+}$ SCs 43 ± 8.2 vs healthy CD3 $^{+}$ SCs 37 ± 3.2 average area). The decreased expression of Ago2 and FXR1 in infiltrating T cells was confirmed using mRNA expression analysis for both these proteins (Fig.

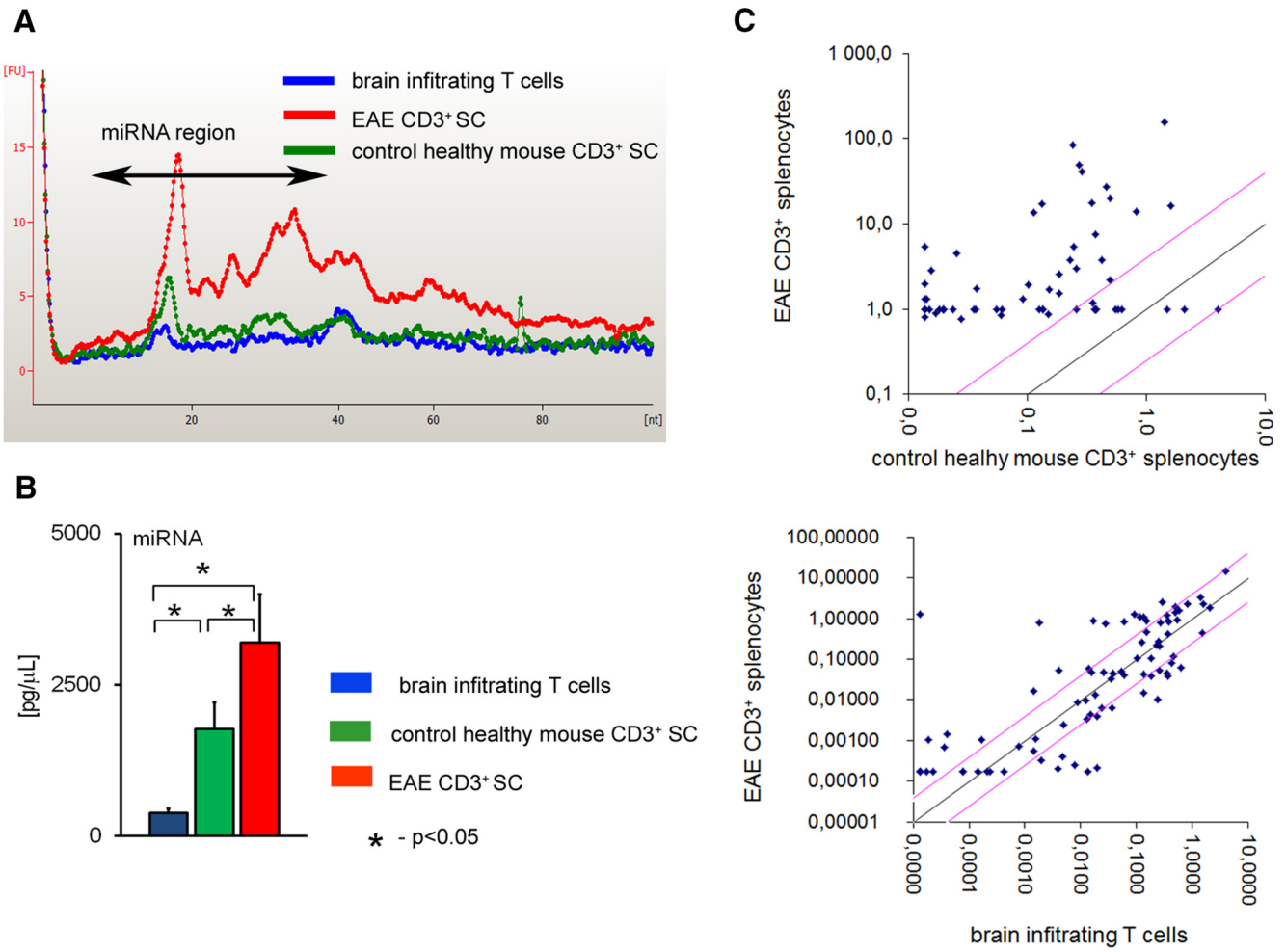

Figure 9. Upregulation of global miRNA level in EAE CD3 $^+$ SCs and downregulation of global miRNA level in EAE brain-infiltrating T cells. ***A***, miRNA region defined arbitrarily (range 10 – 40 nt). Data from one of four experiments performed is shown. ***B***, Average global miRNA concentration ± SD in EAE CD3 $^+$ SCs versus control healthy mouse CD3 $^+$ SCs and brain-infiltrating T cells. ***C***, miRNA profiling of control healthy mouse CD3 $^+$ SCs, EAE CD3 $^+$ SCs, and brain-infiltrating T cells. The majority of analyzed miRNAs are overexpressed in EAE CD3 $^+$ SCs compared with healthy control mouse SCs (top) and the majority of miRNA from brain-infiltrating T cells showed decreased expression compared with EAE CD3 $^+$ SCs (bottom).

6*B*). In EAE brain-infiltrating T cells, qPCR analysis showed downregulation of Ago2 (fold difference decreased by 10.2 ± 1.87) and FXR1 (decreased by 7.4 ± 1.36) compared with EAE CD3 $^+$ SCs (Fig. 6*B*).

Ago2 and FXR1 expression in EAE CD3 $^+$ SCs is increased

Apart from downregulation of Ago2 and FXR1 in brain-infiltrating T cells, we observed marked upregulation of these proteins in CD3 $^+$ SCs of EAE animals. To confirm that Ago2 and FXR1 expression were increased in RISC assembly in CD3 $^+$ SCs of EAE mice, we assessed the amount of Ago2 and FXR1 in complexes with GW182 in SCs of EAE and control mice. In immunoprecipitation experiments, we detected significantly higher expression of Ago2 and FXR1 in complexes with GW182 in EAE compared with control mice (Ago2 with GW182 3887 ± 332 vs control 301 ± 42; FXR1 with GW182 7498 ± 804 vs 2501 ± 603 AVG; Fig. 7*A*,*B*). Furthermore, the Ago2 that coimmunoprecipitated with FXR1 in EAE SCs showed a more intense signal (3005 ± 465 vs control 1099 ± 173 AVG; Fig. 7*C*). The spin-confocal microscopy confirmed a higher amount of FXR1 colocalized with Ago2 in CD3 $^+$ SCs from EAE mice compared with EAE brain-infiltrating T cells, as well as the absence of colocalization in control CD3 $^+$ SCs (Fig. 8*A*). In addition, qPCR analysis showed in EAE CD3 $^+$ SCs significant upregulation of Ago2 (fold difference 9.7 ± 1.97) and FXR1 (fold difference 6.3 ± 1.65) compared with healthy CD3 $^+$ SCs (Fig. 7*D*). These results indicate inadequate (diverse) composition of RISC in SCs of EAE animals as opposed to brain-infiltrating T cells.

Dysregulation of miRNAs in EAE infiltrating T lymphocytes

To explore the role of inadequate RISC protein composition in the regulation of miRNA machinery in EAE brain-infiltrating autoreactive T cells, we analyzed miRNA expression in T cells isolated from EAE brain tissue. Total RNA was measured and used for normalization of the miRNA expression in T cells. In relation to total RNA, the global miRNA level was decreased in T cells derived from brain tissue of EAE animals at the peak of the disease compared with global miRNA levels in SCs from the same EAE animals (378 ± 94.8 vs 3198 ± 768.6 pg/µl; Fig. 9*A*,*B*). The infiltrating T-cell-derived global miRNA level was also decreased, albeit at a lower rate, compared with the global miRNA expression pattern from control SCs derived from healthy mice (378 ± 94.8 vs 1772 ± 431.9 pg/µl; Fig. 9*B*). We observed that the global miRNA level in SCs from EAE mice was significantly higher than that inSCs of control healthy mice. We analyzed further a panel of 86 miRNAs associated with autoimmunity and inflammation in

Table 2. Fold differences in relative miRNA expression between EAE brain-infiltrating T cells and healthy or EAE mice CD3 $^{+}$ SCs

		Fold change		
miRNA	NCBI accession no.	EAE T SC/healthy mouse T SC	EAE-infiltrating T cells/EAE T SC	Effector cells
let-7a-5p	MIMAT0000521	59.02	−97.34	
let-7b-5p	MIMAT0000522	16.66	−1.83	
let-7c-5p	MIMAT0000523	10.91	−3.74	
let-7d-5p	MIMAT0000383	22.20	1.10	
let-7e-5p[a]	MIMAT0000524	36.13	*−52.62*	Positive regulate Th1
let-7f-5p[b]	MIMAT0000525	402.87	−77.84	Negative regulate Th17
let-7g-5p	MIMAT0000121	40.43	3.95	
let-7i-5p[c]	MIMAT0000122	13.91	−4.86	Positive regulate Treg
miR-106a-5p	MIMAT0000385	6.72	−10.02	
miR-106b-5p[a]	MIMAT0000386	2.82	−135.56	Modulates the TGF-β signaling pathway
miR-1192	MIMAT0005850	13.44	13.16	
miR-126a-5p[a]	MIMAT0000137	23.28	−10.33	Positive regulate Th diferentation
miR-128-3p[a]	MIMAT0000140	22.99	−11.37	Positive regulate Th1 and negative Th2
miR-130a-3p	MIMAT0000141	53.84	−6.03	
miR-130b-3p	MIMAT0000387	44.04	4.12	
miR-135a-5p	MIMAT0000147	33.84	−1.23	
miR-140-5p	MIMAT0000151	18.41	−1.08	
miR-144-3p	MIMAT0000156	41.50	−90.42	
miR-155-5p[a]	MIMAT0000165	119.82	9.44	Positive regulate Th1, Th17, Treg, and negative Th2
miR-15a-5p[c]	MIMAT0000526	8.00	2.12	Positive regulate Treg
miR-15b-5p	MIMAT0000124	17.19	2.76	
miR-16-5p	MIMAT0000527	10.33	1.39	
miR-17-5p[b]	MIMAT0000649	11.65	−1.26	Positive regulate Th1 and negative Treg
miR-181a-5p[b]	MIMAT0000210	50.74	−59.55	Intrinsic modulator of T-cell sensitivity and selection
miR-181b-5p[b]	MIMAT0000673	147.69	1.02	Involved in class switch recombination in B-cell
miR-181c-5p	MIMAT0000674	42.19	−3.74	
miR-181d-5p	MIMAT0004324	102.83	3.14	
miR-182-5p[b]	MIMAT0000211	43.84	11.48	Induced by IL-2 promotes clonal expansion of activated CD4 cells
miR-186-5p[a]	MIMAT0000215	45.20	−1.37	
miR-195a-5p	MIMAT0000225	102.60	2.31	
miR-19a-3p	MIMAT0000651	50.19	−7.74	
miR-19b-3p[b]	MIMAT0000513	20.55	−9.49	Positive regulate Th1 and negative Treg
miR-200c-3p	MIMAT0000657	53.84	−2.01	
miR-20a-5p[b]	MIMAT0000529	9.06	−5.10	
miR-20b-5p	MIMAT0003187	8.22	−1.73	
miR-221-3p	MIMAT0000669	73.84	−3.77	
miR-222-3p	MIMAT0000670	127.38	1.87	
miR-23a-3p[b]	MIMAT0000532	111.84	−8.86	
miR-23b-3p	MIMAT0000125	128.10	8.22	
miR-26a-5p[b]	MIMAT0000533	122.48	2.86	
miR-26b-5p[b]	MIMAT0000534	256.21	−22.93	
miR-27a-3p	MIMAT0000537	16.87	−1.04	
miR-27b-3p[a]	MIMAT0000126	18.89	1.05	Positive regulate Th1 and negative Th2
miR-291a-3p	MIMAT0000368	42.84	1.21	
miR-294-3p	MIMAT0000372	40.42	−1.35	
miR-295-3p	MIMAT0000373	31.24	7.53	
miR-29a-3p[b]	MIMAT0000535	1.62	−9.99	Negative regulate Th1
miR-29b-3p[b]	MIMAT0000127	7.45	−9.02	Negative regulate Th1
miR-29c-3p	MIMAT0000536	59.36	−3.98	
miR-301a-3p[c]	MIMAT0000379	28.11	2.11	Positive regulate Th17
miR-301b-3p	MIMAT0004186	47.02	1.22	
miR-302b-3p	MIMAT0003374	33.14	13.16	
miR-302d-3p	MIMAT0003377	22.89	19.24	
miR-30a-5p	MIMAT0000128	2.65	2.24	
miR-30b-5p	MIMAT0000130	2.70	1.11	
miR-30c-5p	MIMAT0000514	4.48	2.95	
miR-30d-5p	MIMAT0000515	11.22	3.01	
miR-30e-5p	MIMAT0000248	2.75	2.42	
miR-322-5p	MIMAT0000548	16.49	−1.48	
miR-326-3p[a]	MIMAT00002107	73.84	−13.16	Positive regulate Th17
miR-338-5p	MIMAT0004647	73.84	−1.09	
miR-340-5p[c]	MIMAT0004651	27.48	−5.85	Positive regulate Th1 and negative Th2
miR-350-3p	MIMAT0000605	67.36	−3.45	
miR-369-3p	MIMAT0003186	52.24	13.16	
miR-384-5p	MIMAT0004745	44.81	56.28	
miR-410-3p	MIMAT0001091	33.09	13.16	
miR-429-3p	MIMAT0001537	21.59	−1.38	

(*Table Continues*)

Table 2. Continued

miRNA	NCBI accession no.	Fold change		
		EAE T SC/healthy mouse T SC	EAE-infiltrating T cells/EAE T SC	Effector cells
miR-466d-3p	MIMAT0004931	21.24	12.91	
miR-466k	MIMAT0005845	11.32	15.40	
miR-495-3p	MIMAT0003456	31.21	13.16	
miR-497-5p[a]	MIMAT0003453	53.91	−2.69	Positive regulate CD8
miR-568	MIMAT0004892	21.34	13.16	
miR-590-3p	MIMAT0004896	33.12	13.16	
miR-669 h-3p	MIMAT0005842	22.94	−32.11	
miR-669k-3p	MIMAT0005831	25.77	−2.38	
miR-694	MIMAT0003474	34.34	10.06	
miR-712-5p	MIMAT0003502	53.09	−1.24	
miR-721	MIMAT0003515	33.11	13.16	
miR-743a-3p	MIMAT0004238	45.04	13.16	
miR-743b-3p	MIMAT0004840	30.09	13.16	
miR-876-3p	MIMAT0004855	23.13	13.16	
miR-9-5p	MIMAT0000142	39.88	6.48	
miR-93-5p	MIMAT0000540	−7.45	−3.14	
miR-98-5p	MIMAT0000545	−63.00	−63.00	

[a]miRNAs associated with in EAE/SM pathogenesis and autoimmune inflammation.

[b]miRNAs associated with autoimmune inflammation by enhancing inflammatory T-cells developed.

[c]miRNAs associated with EAE or MS pathogenesis.

brain-infiltrating T cells and in $CD3^+$ SCs from EAE and healthy mice using qRT-PCR. This allowed us to trace the dynamics of individual miRNA and gradient change during EAE (Fig. 9*C*, Table 2). We found that the majority of analyzed miRNAs were decreased in brain-infiltrating T cells (Fig. 9*C*), whereas in $CD3^+$ SCs from EAE mice, the same miRNAs were increased (Fig. 9*C*). This pattern of miRNA expression allowed us to trace the dynamics of individual miRNA changes during EAE development. The most highly downregulated miRNAs in infiltrating T cells were let-7a-5p, let-7e-5p, let-7f-5p, 106b-5p, 144-3p, and 188a-5p, with a 100-fold decrease compared with SCs from EAE mice.

Discussion

The role of miRNAs in autoimmunity, including EAE, is currently under intense investigation (Sethi et al., 2013). Here, we present data that strongly support the conclusion that global miRNA expression in brains from mice with EAE is regulated by the availability of Ago2, a component of RISCs. Diminished Ago2 expression was found in OLs, the target cells of the autoimmune attack in EAE, as well as in brain-infiltrating effector T lymphocytes. We also found decreased Ago2 and FXR1 presence in RISCs, as well as deficiencies in the formation of Ago2/GW182 and Ago2/FXR1 complexes, in T cells and OLs isolated from EAE brain tissue. Decreased expression of Ago2 and FXR1 correlated with global downregulation of miRNA in both populations of cells.

Mammalian miRNAs are known to be regulated at both the transcriptional and posttranscriptional level. Although many mechanisms of miRNA regulation have been identified, the Ago family of proteins are considered to play a critical role in regulating miRNA homeostasis and to function as the rate-limiting step for miRNA maturation (Diederichs and Haber, 2007; Johnston and Hutvagner, 2011). Overexpression of any of the four Ago (1–4) proteins leads to an increased expression of mature miRNA (Diederichs and Haber, 2007; Johnston and Hutvagner, 2011) and, in Ago2-knock-out mice (disrupted gene for Eif2c2), lower total miRNA expression has been observed (Morita et al., 2007). Because Ago2 represents an important regulatory checkpoint for miRNAs, it was critically important to show that Ago2 expression was downregulated in activated T cells infiltrating brain tissue. Our data clearly indicate a diminished presence of Ago2 associated with the RISC complex, deficient formation of Ago2 complexes with FXR1 and GW182, and reduced miRNA binding to RISC. Therefore, reduced expression of Ago2 correlated with inhibition of miRNA expression in infiltrating T cells in EAE CNS tissue.

It has been shown previously that activation of T cells leads to global posttranscriptional downregulation of mature miRNA that is dependent on Ago2 activity, suggesting that mature miRNA inhibition during cell activation allows for active reprogramming of the pattern of miRNA expression in differentiated effector cells (Bronevetsky et al., 2013). Indeed, naive T cells and various Th cell lineages have been found to express profound differences in the expression patterns of miRNA (Sethi et al., 2013). Therefore, our findings on miRNA inhibition in polarized effector T cells infiltrating EAE brain tissue are consistent with the hypothesis that activation-induced miRNA downregulation promotes acquisition of T-cell effector functions by diminishing the repression of genes involved in T-cell differentiation (Bronevetsky et al., 2013). The function of Ago2 protein can also be modulated in response to specific binding of FXR1, leading to enhanced translation by Ago2/FXR1. Specifically, it has been shown that Ago2 and FXR1 bind to the AU-rich element in the 3′-UTR of TNF-α mRNA, activating its translation within immune cells (Vasudeva and Steitz, 2007). Collectively, our data suggest that activation of infiltrating T cells in EAE culminates in inhibition of Ago2 and FXR1 proteins that correlates with decreased miRNA expression, allowing for active mRNA synthesis. Consistent with this conclusion, it has been shown that, although Ago2-deficient T cells are phenotypically normal before activation, they are more prone to differentiate into cytokine-secreting cells after TCR stimulation (Bronevetsky et al., 2013). Infiltrating T cells in EAE secrete a wide range of proinflammatory cytokines that have been shown to contribute to the inflammatory pathology of this disease (Jurewicz et al., 2005).

The data on global inhibition of miRNAs in activated T cells in EAE brain were supported by the data from qRT-PCR arrays that analyzed the expression of 86 miRNAs in confirmatory experiments with brain-infiltrating T cells. We found that the majority

of miRNAs that are associated with the inflammatory response and autoimmunity, such as let-7e-5p, 126a-5p, 128-3p, 155-5p, 186a-5p, 340-5p, and 497-5p (Sethi et al., 2013), were decreased in EAE brains compared with miRNA profiling in EAE SCs. The miRNA profile in $CD3^+$ SCs from EAE animals showed significantly higher expression compared with SCs from healthy mice. Previous studies have shown that, on average, activated T cells demonstrate increased production of mRNA by 10-fold (Heap et al., 2010; Zhao et al., 2014), which allows for the translation of a number of specific immune factors that determine their immune function. Furthermore, in MS patients, the level of miRNA-340 was found to be increased in peripheral memory $CD4^+$ cells, thereby favoring a proinflammatory Th1 response (Guerau-de-Arellano et al., 2012). The gradient of miRNA expression that we observed between healthy and EAE SCs suggests active involvement of miRNA in T-cell polarization toward effector cells in EAE. Furthermore, diminished miRNA expression in EAE brain-infiltrating T cells suggests that mature, polarized effector T cells do not require extensive posttranscriptional regulation.

miRNAs also play an important role in OL differentiation and survival (Budde et al., 2010; Dugas et al., 2010; Wang and Cambi, 2012; Zheng et al., 2012; de Faria et al., 2012). Of particular interest is the finding that ablation of DICER in OLs leads to inhibition of pre-miRNA generation, resulting in demyelination and inflammation, features characteristic of EAE and MS pathology (Dugas et al., 2010; Zhao et al., 2010). In addition, conditional knockout of the miRNA 17–92 cluster inhibits OL proliferation and causes reduction in OL numbers (Budde et al., 2010). These results strongly support the concept that miRNAs regulate myelin stability (Shin et al., 2012). The results of our study showing that during EAE global miRNA expression in OLs is diminished are consistent with this hypothesis. In addition, our data showing that miRNA inhibition in OLs during EAE is linked with downregulation of Ago2 and FXR1 proteins and dysregulation of RISC assembly formation, as demonstrated by impaired ability to create Ago2/GW182 and Ago2/FXR1 complexes, indicates that Ago2 and FXR1 might play a regulatory role for miRNAs in OLs similar to T cells. To explore further the role of disruption of RISC protein composition and diminished Ago2 and FXR1 in OLs on miRNA expression, we examined miRNA profiling in these cells. We found that the majority of miRNAs were downregulated (56 of 86), including the miRNA-17-92 cluster (miRNAs 20a and 92a-1). Recent studies have shown that the miR-17-92 cluster is essential for the differentiation, proliferation, and/or survival of OLs (Budde et al., 2010). In addition, miR-338-3p and -5, which we found to be strikingly decreased (nearly 10-fold) in EAE OLs, have been implicated in the regulation of OPC differentiation and OL myelin gene expression (Dugas et al., 2010).

The mechanism of Ago2 downregulation in infiltrating T cells and OLs is not clear. Altered Ago2 expression revealed that Ago2 is a limiting factor that determines miRNA abundance and global miRNA expression levels (Diederichs and Haber, 2007; O'Carroll et al., 2007; Lund et al., 2011; Bronevetsky et al., 2013). Ago2 actively participates in miRNA biogenesis and increases miRNA expression by stabilizing the effect of Ago2 on mature miRNA in a silencing-independent manner (Winter and Diederichs, 2011). Cells lacking Ago2 show profound inhibition and reduced half-lives of miRNA (Winter and Diederichs, 2011). Accordingly, overexpression of Ago2 decelerates miRNA degradation (Winter and Diederichs, 2011). In our study, low miRNA levels, which are associated with decreased Ago, might point to destabilization of Ago2 in EAE brain. The unstable unloaded form of Ago is more sensitive to degradation by the ubiquitin-proteasomal system (Rybak et al., 2009; Bronevetsky et al., 2013). It was suggested that miRNA availability controls Ago2 levels (Hauptmann and Meister 2013; Smibert et al., 2013). Dicer-deficient fibroblasts show reduced Ago2 expression caused by enhanced proteasome-mediated Ago2 degradation. It has also been suggested that phosphorylation of Ago2 impairs loading of miRNA onto Ago2 leading to Ago2 destabilization (Shen et al., 2013). However, several other signaling pathways might also be involved in Ago2 regulation, such as protein prolyl hydroxylation (Qi et al., 2008), phosphorylation (Zeng et al., 2008; Rüdel et al., 2011; Horman et al., 2013), ubiquitination, poly-ADP-ribosylation (Leung et al., 2011, Leung and Sharp, 2013), autophagy degradation (Gibbings et al., 2012), or change in Ago2 localization (Jee and Lai, 2014). It also remains possible that the inflammatory environment contributes to this phenomenon because we observed downregulation of miRNA biogenesis related to decreased RISC formation during EAE in CNS endogenous cells, OLs, and brain-infiltrating T cells. Based on some initial studies, it has also been proposed that a genetic association of miRNA and inflammatory pathology might also exist (Jennewein et al., 2010), but these data are limited in regard to inflammatory disorders.

In summary, our findings suggest that Ago2 and inadequate RISC assembly might be critical factors regulating miRNA expression, which contributes to the development of autoimmune demyelination in EAE and MS. Diminished Ago2 expression allows for decreased translational inhibition and the expression of a proinflammatory profile in brain-infiltrating T cells, whereas diminished Ago2 expression in OLs contributes to demyelination and OL loss. Therefore, Ago2-mediated miRNA abnormalities might contribute to MS pathology by multiple mechanisms and modification of mechanisms that regulate the level of Ago2 may be a significant factor in future therapies.

References

Bhattacharyya SN, Filipowicz W (2007) Argonautes and company: sailing against the wind. Cell 128:1027–1028. CrossRef Medline

Boudreau RL, Jiang P, Gilmore BL, Spengler RM, Tirabassi R, Nelson JA, Ross CA, Xing Y, Davidson BL (2014) Transcriptome-wide discovery of microRNA binding sites in human brain. Neuron 81:294–305. CrossRef Medline

Breving K, Esquela-Kerscher A (2010) The complexities of microRNA regulation: mirandering around the rules. Int J Biochem Cell Biol 42:1316–1329. Medline

Bronevetsky Y, Villarino AV, Eisley CJ, Barbeau R, Barczak AJ, Heinz GA, Kremmer E, Heissmeyer V, McManus MT, Erle DJ, Rao A, Ansel KM (2013) T cell activation induces proteasomal degradation of Argonaute and rapid remodeling of the microRNA repertoire. J Exp Med 210:417–432. CrossRef Medline

Budde H, Schmitt S, Fitzner D, Opitz L, Salinas-Riester G, Simons M (2010) Control of oligodendroglial cell number by the miR-17-92 cluster. Development 137:2127–2132. CrossRef Medline

Cox MB, Cairns MJ, Gandhi KS, Carroll AP, Moscovis S, Stewart GJ, Broadley S, Scott RJ, Booth DR, Lechner-Scott; ANZgene Multiple Sclerosis Genetics Consortium (2010) MicroRNAs miR-17 and miR-20a inhibit T cell activation genes and are under-expressed in MS whole blood. PLoS One 5:e12132. CrossRef Medline

de Faria O Jr, Cui QL, Bin JM, Bull SJ, Kennedy TE, Bar-Or A, Antel JP, Colman DR, Dhaunchak AS (2012) Regulation of miRNA 219 and miRNA clusters 338 and 17–92 in oligodendrocytes. Front Genet 3:46. Medline

Diederichs S, Haber DA (2007) Dual role for argonautes in microRNA processing and posttranscriptional regulation of microRNA expression. Cell 131:1097–1108. CrossRef Medline

Dima AA, Elliott JT, Filliben JJ, Halter M, Peskin A, Bernal J, Kociolek M, Brady MC, Tang HC, Plant AL (2011) Comparison of segmentation al-

gorithms for fluorescence microscopy images of cells. Cytometry A 79: 545–559. Medline

Dugas JC, Cuellar TL, Scholze A, Ason B, Ibrahim A, Emery B, Zamanian JL, Foo LC, McManus MT, Barres BA (2010) Dicer1 and miR-219 are required for normal oligodendrocyte differentiation and myelination. Neuron 65:597–611. CrossRef Medline

Eulalio A, Tritschler F, Izaurralde E (2009) The GW182 protein family in animal cells: new insights into domains required for miRNA-mediated gene silencing. RNA 15:1433–1442. CrossRef Medline

Fabian MR, Sonenberg N, Filipowicz W (2010) Regulation of mRNA translation and stability by microRNAs. Annu Rev Biochem 79:351–379. CrossRef Medline

Gibbings D, Mostowy S, Jay F, Schwab Y, Cossart P, Voinnet O (2012) Selective autophagy degrades DICER and AGO2 and regulates miRNA activity. Nat Cell Biol 14:1314–1321. CrossRef Medline

Guan H, Fan D, Mrelashvili D, Hao H, Singh NP, Singh UP, Nagarkatti PS, Nagarkatti M (2013) MicroRNA let-7e is associated with the pathogenesis of experimental autoimmune encephalomyelitis. Eur J Immunol 43: 104–114. CrossRef Medline

Guerau-de-Arellano M, Smith KM, Godlewski J, Liu Y, Winger R, Lawler SE, Whitacre CC, Racke MK, Lovett-Racke AE (2011) Micro-RNA dysregulation in multiple sclerosis favours pro-inflammatory T-cell-mediated autoimmunity. Brain 134:3578–3589. CrossRef Medline

Guerau-de-Arellano M, Alder H, Ozer HG, Lovett-Racke A, Racke MK (2012) miRNA profiling for biomarker discovery in multiple sclerosis: from microarray to deep sequencing. J Neuroimmunol 248:32–39. CrossRef Medline

Hansel NN, Cheadle C, Diette GB, Wright J, Thompson KM, Barnes KC, Georas SN (2008) Analysis of $CD4^+$ T-cell gene expression in allergic subjects using two different microarray platforms. Allergy 63:366–369. CrossRef Medline

Hauptmann J, Meister G (2013) Argonaute regulation: two roads to the same destination. Dev Cell 25:553–554. CrossRef Medline

Heap GA, Yang JH, Downes K, Healy BC, Hunt KA, Bockett N, Franke L, Dubois PC, Mein CA, Dobson RJ, Albert TJ, Rodesch MJ, Clayton DG, Todd JA, van Heel DA, Plagnol V (2010) Genome-wide analysis of allelic expression imbalance in human primary cells by high-throughput transcriptome resequencing. Hum Mol Genet 19:122–134. CrossRef Medline

Horman SR, Janas MM, Litterst C, Wang B, MacRae IJ, Sever MJ, Morrissey DV, Graves P, Luo B, Umesalma S, Qi HH, Miraglia LJ, Novina CD, Orth AP (2013) Akt-mediated phosphorylation of argonaute 2 downregulates cleavage and upregulates translational repression of MicroRNA targets. Mol Cell 50:356–367. CrossRef Medline

Jakymiw A, Lian S, Eystathioy T, Li S, Satoh M, Hamel JC, Fritzler MJ, Chan EK (2005) Disruption of GW bodies impairs mammalian RNA interference. Nat Cell Biol 7:1267–1274. CrossRef Medline

Jee D, Lai EC (2014) Alteration of miRNA activity *via* context-specific modifications of Argonaute proteins. Trends Cell Biol 24:546–553. CrossRef Medline

Jennewein C, von Knethen A, Schmid T, Brüne B (2010) MicroRNA-27b contributes to lipopolysaccharide-mediated peroxisome proliferator-activated receptor gamma (PPARgamma) mRNA destabilization. J Biol Chem 285:11846–11853. CrossRef Medline

Johnston M, Hutvagner G (2011) Posttranslational modification of Argonautes and their role in small RNA-mediated gene regulation. Silence 2:5. CrossRef Medline

Junker A (2011) Pathophysiology of translational regulation by microRNAs in multiple sclerosis. FEBS Lett 585:3738–3746. CrossRef Medline

Junker A, Krumbholz M, Eisele S, Mohan H, Augstein F, Bittner R, Lassmann H, Wekerle H, Hohlfeld R, Meinl E (2009) MicroRNA profiling of multiple sclerosis lesions identifies modulators of the regulatory protein CD47. Brain 132:3342–3352. CrossRef Medline

Jurewicz A, Matysiak M, Tybor K, Kilianek L, Raine CS, Selmaj K (2005) Tumour necrosis factor-induced death of adult human oligodendrocytes is mediated by apoptosis inducing factor. Brain 128:2675–2688. CrossRef Medline

Jurynczyk M, Jurewicz A, Raine CS, Selmaj K (2008) Notch3 inhibition in myelin-reactive T cells down-regulates protein kinase C theta and attenuates experimental autoimmune encephalomyelitis. J Immunol 180: 2634–2640. CrossRef Medline

Kawamata T, Tomari Y (2010) Making RISC. Trends Biochem Sci 35:368–376. CrossRef Medline

Koenning M, Jackson S, Hay CM, Faux C, Kilpatrick TJ, Willingham M, Emery B (2012) Myelin gene regulatory factor is required for maintenance of myelin and mature oligodendrocyte identity in the adult CNS. J Neurosci 32:12528–12542. CrossRef Medline

Kuhn CD, Joshua-Tor L (2013) Eukaryotic Argonautes come into focus. Trends Biochem Sci 38:263–271. CrossRef Medline

Lerner M, Lundgren J, Akhoondi S, Jahn A, Ng HF, Akbari Moqadam F, Oude Vrielink JA, Agami R, Den Boer ML, Grandér D, Sangfelt O (2011) miRNA-27a controls FBW7/hCDC4-dependent cyclin E degradation and cell cycle progression. Cell Cycle 10:2172–2183. CrossRef Medline

Leung AK, Sharp PA (2013) Quantifying Argonaute proteins in and out of GW/P-bodies: implications in microRNA activities. Adv Exp Med Biol 768:165–182. CrossRef Medline

Leung AK, Vyas S, Rood JE, Bhutkar A, Sharp PA, Chang P (2011) Poly(ADP-ribose) regulates stress responses and microRNA activity in the cytoplasm. Mol Cell 42:489–499. CrossRef Medline

Liu J, Carmell MA, Rivas FV, Marsden CG, Thomson JM, Song JJ, Hammond SM, Joshua-Tor L, Hannon GJ (2004) Argonaute2 is the catalytic engine of mammalian RNAi. Science 305:1437–1441. CrossRef Medline

Liu J, Rivas FV, Wohlschlegel J, Yates JR 3rd, Parker R, Hannon GJ (2005) A role for the P-body component GW182 in microRNA function. Nat Cell Biol 7:1261–1266. CrossRef Medline

Lund E, Sheets MD, Imboden SB, Dahlberg JE (2011) Limiting Ago protein restricts RNAi and microRNA biogenesis during early development in *Xenopus laevis.* Genes Dev 25:1121–1131. CrossRef Medline

Ma X, Zhou J, Zhong Y, Jiang L, Mu P, Li Y, Singh N, Nagarkatti M, Nagarkatti P (2014) Expression, regulation and function of microRNAs in multiple sclerosis. Int J Med Sci 11:810–818. CrossRef Medline

Moore GR, Traugott U, Farooq M, Norton WT, Raine CS (1984a) Experimental autoimmune encephalomyelitis: augmentation of demyelination by different myelin lipids. Lab Invest 51:416–424. Medline

Moore GR, Traugott U, Raine CS (1984b) Survival of oligodendrocytes in chronic relapsing experimental autoimmune encephalomyelitis. J Neurol Sci 65:137–145. CrossRef Medline

Morita S, Horii T, Kimura M, Goto Y, Ochiya T, Hatada I (2007) One Argonaute family member, Eif2c2 (Ago2), is essential for development and appears not to be involved in DNA methylation. Genomics 89:687–696. CrossRef Medline

Mycko MP, Cichalewska M, Machlanska A, Cwiklinska H, Mariasiewicz M, Selmaj KW (2012) MicroRNA-301a regulation of a T-helper 17 immune response controls autoimmune demyelination. Proc Natl Acad Sci U S A 109:E1248–E1257. CrossRef Medline

O'Carroll D, Mecklenbrauker I, Das PP, Santana A, Koenig U, Enright AJ, Miska EA, Tarakhovsky A (2007) A Slicer-independent role for Argonaute 2 in hematopoiesis and the microRNA pathway. Genes Dev 21: 1999–2004. CrossRef Medline

Ode F Jr, Moore CS, Kennedy TE, Antel JP, Bar-Or A, Dhaunchak AS (2012) MicroRNA dysregulation in multiple sclerosis. Front Genet 3:311. CrossRef Medline

Pauley KM, Eystathioy T, Jakymiw A, Hamel JC, Fritzler MJ, Chan EK (2006) Formation of GW bodies is a consequence of microRNA genesis. EMBO Rep 7:904–910. CrossRef Medline

Piccio L, Rossi B, Colantonio L, Grenningloh R, Gho A, Ottoboni L, Homeister JW, Scarpini E, Martinello M, Laudanna C, D'Ambrosio D, Lowe JB, Constantin G (2005) Efficient recruitment of lymphocytes in inflamed brain venules requires expression of cutaneous lymphocyte antigen and fucosyltransferase-VII. J Immunol 174:5805–5813. CrossRef Medline

Pillai RS, Bhattacharyya SN, Artus CG, Zoller T, Cougot N, Basyuk E, Bertrand E, Filipowicz W (2005) Inhibition of translational initiation by Let-7 MicroRNA in human cells. Science 309:1573–1576. CrossRef Medline

Ponomarev ED, Veremeyko T, Barteneva N, Krichevsky AM, Weiner HL (2011) MicroRNA-124 promotes microglia quiescence and suppresses EAE by deactivating macrophages via the C/EBP-α-PU.1 pathway. Nat Med 17:64–70. CrossRef Medline

Qi HH, Ongusaha PP, Myllyharju J, Cheng D, Pakkanen O, Shi Y, Lee SW, Peng J, Shi Y (2008) Prolyl 4-hydroxylation regulates Argonaute 2 stability. Nature 455:421–424. CrossRef Medline

Rüdel S, Wang Y, Lenobel R, Körner R, Hsiao HH, Urlaub H, Patel D, Meister

G (2011) Phosphorylation of human Argonaute proteins affects small RNA binding. Nucleic Acids Res 39:2330–2343. CrossRef Medline

Rybak A, Fuchs H, Hadian K, Smirnova L, Wulczyn EA, Michel G, Nitsch R, Krappmann D, Wulczyn FG (2009) The let-7 target gene mouse lin-41 is a stem cell specific E3 ubiquitin ligase for the miRNA pathway protein Ago2. Nat Cell Biol 11:1411–1420. CrossRef Medline

Sethi A, Kulkarni N, Sonar S, Lal G (2013) Role of miRNAs in CD4 T cell plasticity during inflammation and tolerance. Front Genet 4:8. Medline

Shen J, Xia W, Khotskaya YB, Huo L, Nakanishi K, Lim SO, Du Y, Wang Y, Chang WC, Chen CH, Hsu JL, Wu Y, Lam YC, James BP, Liu X, Liu CG, Patel DJ, Hung MC (2013) EGFR modulates microRNA maturation in response to hypoxia through phosphorylation of AGO2. Nature 497:383–387. CrossRef Medline

Shin D, Howng SY, Ptáček LJ, Fu YH (2012) miR-32 and its target SLC45A3 regulate the lipid metabolism of oligodendrocytes and myelin. Neuroscience 213:29–37. CrossRef Medline

Smibert P, Yang JS, Azzam G, Liu JL, Lai EC (2013) Homeostatic control of Argonaute stability by microRNA availability. Nat Struct Mol Biol 20:789–795. CrossRef Medline

Sospedra M, Martin R (2005) Immunology of multiple sclerosis. Annu Rev Immunol 23:683–747. CrossRef Medline

Thamilarasan M, Koczan D, Hecker M, Paap B, Zettl UK (2012) MicroRNAs in multiple sclerosis and experimental autoimmune encephalomyelitis. Autoimmun Rev 11:174–179. CrossRef Medline

Vasudevan S, Steitz JA (2007) AU-rich-element-mediated upregulation of translation by FXR1 and Argonaute 2. Cell 128:1105–1118. CrossRef Medline

Wang E, Cambi F (2012) MicroRNA expression in mouse oligodendrocytes and regulation of proteolipid protein gene expression. J Neurosci Res 90:1701–1712. CrossRef Medline

Winter J, Diederichs S (2011) Argonaute proteins regulate microRNA stability: Increased microRNA abundance by Argonaute proteins is due to microRNA stabilization. RNA Biol 8:1149–1157. CrossRef Medline

Xu W, Liu M, Peng X, Zhou P, Zhou J, Xu K, Xu H, Jiang S (2013) miR-24-3p and miR-27a-3p promote cell proliferation in glioma cells via cooperative regulation of MXI1. Int J Oncol 42:757–766. Medline

Zeng Y, Sankala H, Zhang X, Graves PR (2008) Phosphorylation of Argonaute 2 at serine-387 facilitates its localization to processing bodies. Biochem J 413:429–436. CrossRef Medline

Zhao S, Fung-Leung WP, Bittner A, Ngo K, Liu X (2014) Comparison of RNA-Seq and microarray in transcriptome profiling of activated T cells. PLoS One 9:e78644. CrossRef Medline

Zhao X, He X, Han X, Yu Y, Ye F, Chen Y, Hoang T, Xu X, Mi QS, Xin M, Wang F, Appel B, Lu QR (2010) MicroRNA-mediated control of oligodendrocyte differentiation. Neuron 65:612–626. CrossRef Medline

Zheng K, Li H, Huang H, Qiu M (2012) MicroRNAs and glial cell development. Neuroscientist 18:114–118. CrossRef Medline